CHAPTER 3-- GEOPHYSICS

Geophysical surveys were performed on the SE slope of Snodgrass Mountain in July and October, 2007. In total, about 8870 ft of line were measured on 3 long, parallel lines that each extended SE down the fall line on the SE slope (West Line, 2430 ft; Central Line beneath main lift, 3810 ft; East Line, 2630 ft).

Geophysical surveys often play only a minor, supporting role in landslide investigations, because if drilling access is easy, subsurface cross-sections can be based on abundant boreholes drilled to whatever depth desired. That was not the case at Snodgrass; no roads existed or could be built on most of the mountain, and we were thus limited to using a small, track-mounted, exploratory auger rig. To make up for the limited number of boreholes we could drill (14) and the limited depth penetration (many encountered refusal in the top of bedrock), we turned to seismic refraction surveys to help us interpolate between the drillholes. The resulting seismic refraction tomograms (both P-wave and S-wave) and the vertical shear wave profiling provided two pieces of information the drilling could not: (1) geologic (interpreted) contacts could be traced between boreholes, and (2) geologic conditions could be inferred as deep as 150 ft, or 2-3 times the depth of the average borehole. Because of these advantages, we relied heavily on the seismic tomograms when drawing the geologic cross-sections used in the stability analysis (Chapter 8).

In the present study, we performed two separate campaigns of geophysical data collection with two different contractors in 2007 (Fig. 3.1). These geophysical surveys were performed to supplement the data obtained by previous geophysical surveys and drilling, as to the depth of the landslide deposits (depth to basal failure plane), and the depth to groundwater. From July 7-17, Jim O'Donnell (geophysical consultant, Las Vegas, NV) surveyed 6 semi-contiguous 480-ft spreads on the central geophysical line (Central Line) on the southeastern slopes of Snodgrass Mountain, with Line 1 in the lower end of the Chicken Bone area, and Lines 2-6 extending continuously downslope from Ken's Crux to the top of the Slump Block. These surveys used seismic refraction tomography and ReMi.

Between October 3 and10, Zonge Geosciences (Denver, CO) finished the southern end of the Central Line down to the toe of the Slump Block (five 240 ft-long spreads), and then surveyed 2 new long lines down the lengths of the East Slide/ GHUs 5A and 5B (East Line; twelve 240-ft spreads) and down the axis of the western slide complex/ GHUs 1A, 1B, and 4 (West Line; eleven 240 ft-long spreads). All spreads collected both P-wave and S-wave seismic refraction data. These campaigns and their results are described separately below.

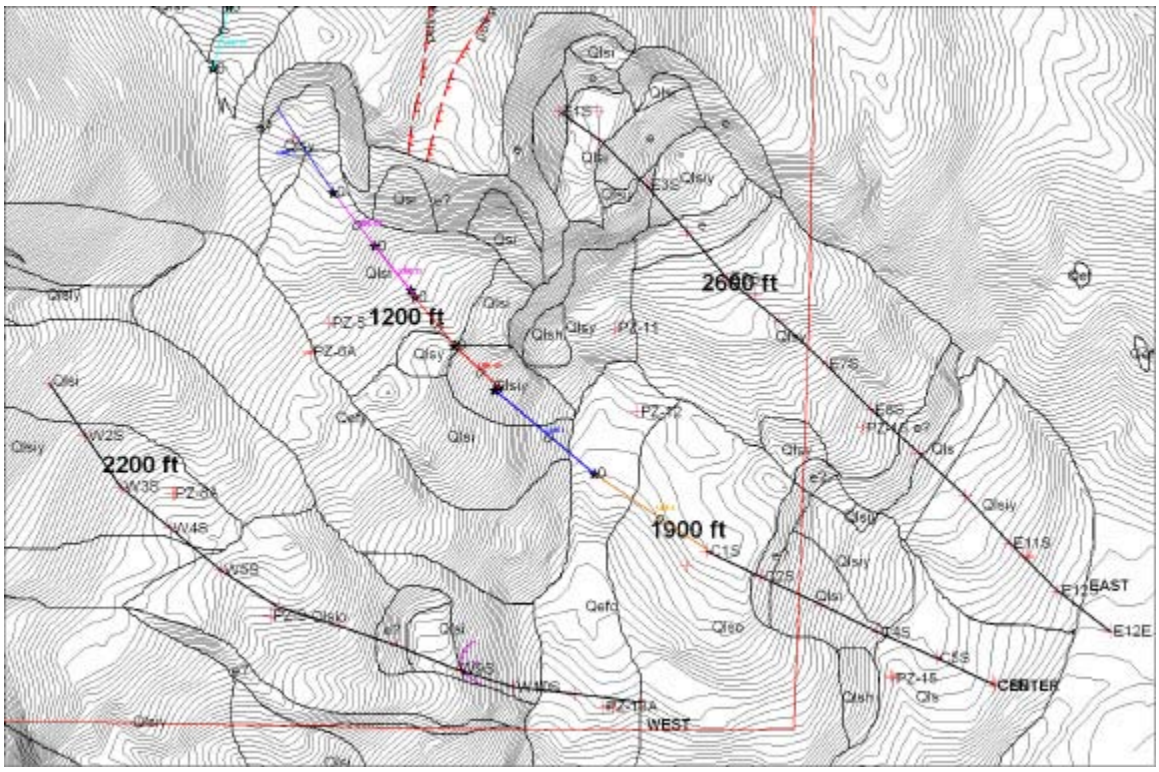

Fig. 3-1 Map of the southeastern slopes of Snodgrass Mountain, showing locations of the geophysical survey lines measured in 2007. Spreads are labeled consecutively from NW to SE on each line (e.g., W2S for the West Line, E7S for the East Line). Red line shows the boundary of the permit area. Landslide polygons with age labels, piezometers, and inclinometers are also shown. Contour interval is 5 ft.

3.0 Previous geophysical studies

In 1984 and 1986 Western Engineers, Inc. performed P-wave seismic refraction surveys at the base of Snodgrass Mountain, south of the Slump Block (Western Engineers, 1984, 1986). The surveys concentrated on both banks of the stream that flows west from the North Village area toward Washington Gulch, where the stream course is constricted by a linear ridge that projects southward from the base of Snodgrass. This ridge was to be the right abutment of a dam proposed by the Mt. Crested Butte Water & Sanitation District.

The 1984 surveys were relatively inconclusive as to the origin of the northern ridge and its suitability as a dam abutment. Western Engineering (1984) did conclude that, in the 7 lines surveyed, a low velocity layer (ca. 925 fps) 6-12 ft thick overlay a moderate velocity layer (ca. 5800 fps). However, it was impossible to say whether the moderate-velocity layer was weathered Mancos Shale, or merely saturated Quaternary deposits.

Due to this ambiguity, 7 additional lines were shot in Sept. 1986, along with several new test pits excavated (Western Engineering, 1986). The 1986

lines confirmed the existence of a thin low velocity layer (unsaturated Quaternary deposits) over a moderate-velocity layer. The moderate-velocity layer was interpreted as saturated material below the water table, usually a Quaternary deposit. In addition, four of the lines detected a high-velocity layer (8744 fps, 11,050 fps, 9762 fps, 10,796 fps) at depths ranging from 27-53 ft. This layer was interpreted as in-situ, "competent" Mancos Shale.

3.1 Methods—O'Donnell Surveys of July 2007

Refraction P-wave Tomography and Refraction Microtremor (ReMi) S-wave surveys were employed at the site; both methods were performed on the same geophone lines, using the same geophone number and spacing. In spite of its name, ReMi is not a refraction method, but becomes extremely powerful when used in conjunction with refraction tomography. Since the same array setup can be used to record ReMi and refraction data, one can use the shear-wave (Vs) and compression wave velocities (Vp) obtained from each method to generate more complete images of the subsurface. In our case, ReMi gives the deeper velocities and maps low-velocity horizons that are missed by refraction, while refraction tomography provides higher resolution at shallower horizons and maps lateral variations along the profile. The two methods are quite complimentary, because the refraction method has greater resolution but suffers from the fundamental problem of a lack of penetration when encountering a lower velocity at depth (velocity inversions**).** The refraction method has difficulty in detecting "hidden layers" (Burger, 1992) such as a high velocity thin layer or a low velocity layer "sandwiched" between two high velocity layers. Such "hidden layers" cause erroneous data interpretation. An improved way to interpret refraction data is through use of refraction tomography with ReMi data, which is able to measure through a velocity inversion.

All seismic data were recorded using 10-Hz geophones consisting of either 24 or 48 geophones with 10 foot spacing. In addition, the seismic data was collected utilizing Seismic Sources Company, 24-48 channel, DAQLink II digital seismograph and data acquisition software Vibroscope V2.30.0. The Vs data were collected at sample rate of two milliseconds for intervals of 25 seconds; while the Vp data were collected at a sample rate of 0.25 milliseconds for 0.5 second. The field crew consisted of a 4 man team which included Jim O'Donnell (geophysicist) and Jim Houda (crew chief).

In general, geophysical methods are much more global in nature than borehole measurements, which only measure rock properties in the borehole or very close to it. Furthermore, the ReMi method is more global than the refraction method as discussed later. Under ideal rock conditions Vp/Vs~1.7, but under soil conditions the ratio can increase dramatically to as much as 10, normally because of a decrease in Vs due to soft soils.

3.1.1 Seismic Refraction Tomography (Vp)

The Vp surveys used active sources which were a slide hammer and small buried explosive charges. In order to analyze the Vp data as a 2D Tomography profile, multiple source points (hit and shot) are made along the line (off the ends too) while the hammer hits were stacked to improve the signal/noise ratio. The other requirements for the analysis are to make the first break picks from the seismic record and know the geometry of the line. In our case we had straight lines but were working on very steep slopes so the elevation changes had to be measured. Each shot point gives a possible number of raypaths, which travel from the shot point to each receiver (geophone). In most cases we had 48 geophones and 5 shot points along a line giving a possible 240 raypaths to measure Vp beneath the line. Each 2D Tomography profile has a corresponding raypath model which shows how well the raypaths covered the model.

The first break picks (Vp arrival travel-time) were made by Jim O'Donnell and subsequently analyzed by Satish K. Pullammanappallil (University of Nevada-Reno), using the latest software developed from Optim LLC SeisOpt®@2-D™ version 5.0. For a more extensive description of the method used see Pullammanappallil and Louie (1994).

3.1.2 Seismic Shear Waves from ReMi (Vs)

The Vs method uses background noise for signal, Rayleigh waves, which are generated from wind and from the drilling operation when active. A big part of the Rayleigh waves are formed from Shear waves and the Shear wave velocities can be obtained from analysis of the ReMi data (Louie, 2001). Actually, the ReMi method is one of three Surface Wave methods used to compute average Vs down to a 100 foot depth which is required by the International Building Code for Geotechnical work (IBC-2000). The other two methods are the better known Spectral Analysis of Surface Waves (SASW) and Multiple Analysis of Surface Waves (MASW). All three methods can be used to compute 1D models as the Vs changes with depth. The big difference between the three methods is ReMi can use Passive Rayleigh waves (background noise) while the other two require an active source such as hammer hits which limit the depth of investigation.

Consequently, when we measure the ReMi data over a line length (in our case L=230 feet or 470 feet), we are getting an average Vs over the entire length of the line. The measured depth is proportional to the line length, the wave length of the Rayleigh wave recorded, and the velocity of the propagating material. The longer wave lengths penetrate deeper and measure to deeper depths than the shorter wave lengths (higher frequencies), which are limited to shallower depths. The wave lengths we encountered were on the order of 30' to 300', which is an indication of the geology we are able to sample.

3.2 Results—Surveys of July 2007 On and Above the Steep Slope Band

3.2.1 Lines 1N and 1S

Lines 1N and 1S lie in the lowest part of the Chicken Bone area (GHU 6), and were surveyed to determine the thickness of the Qlsi mapped there. Each line was ca. 240 ft long, with 1N extending N from borehole PZ-2 and 1S extending south. The uninterpreted P-wave tomogram is shown in Fig. 3-2 and a pseudo 2D ReMi tomogram is shown in Fig. 3.3, based on the vertical ReMi soundings shown in Fig. 3.4.

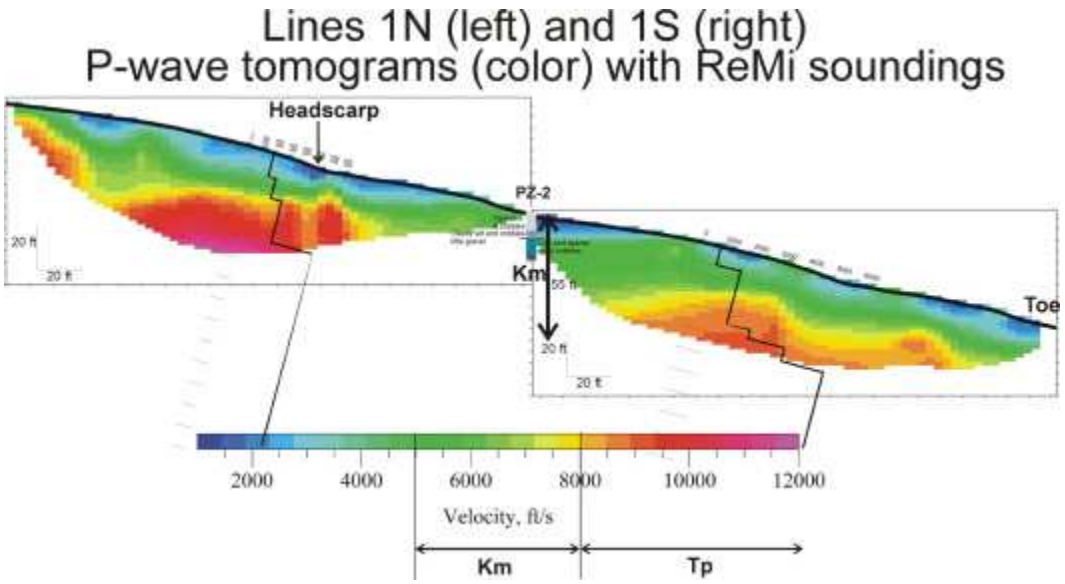

Fig. 3-2. P-wave tomogram, Lines 1N and 1S. The S-wave vertical profile from each line is superimposed.

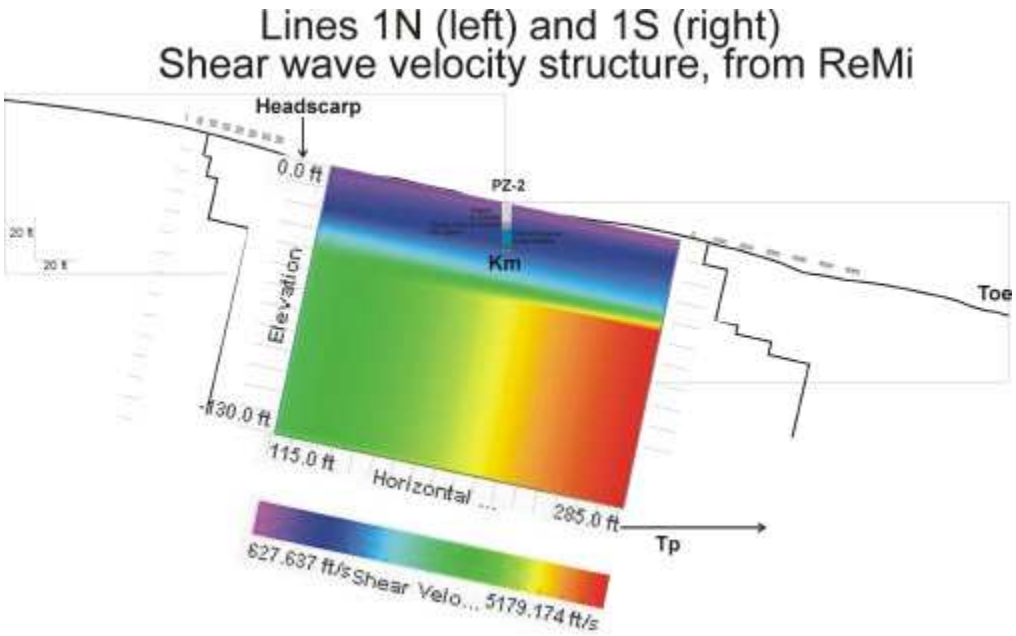

Fig. 3-3. Pseudo 2D S-wave tomogram based on the 2 vertical ReMi soundings.

Title

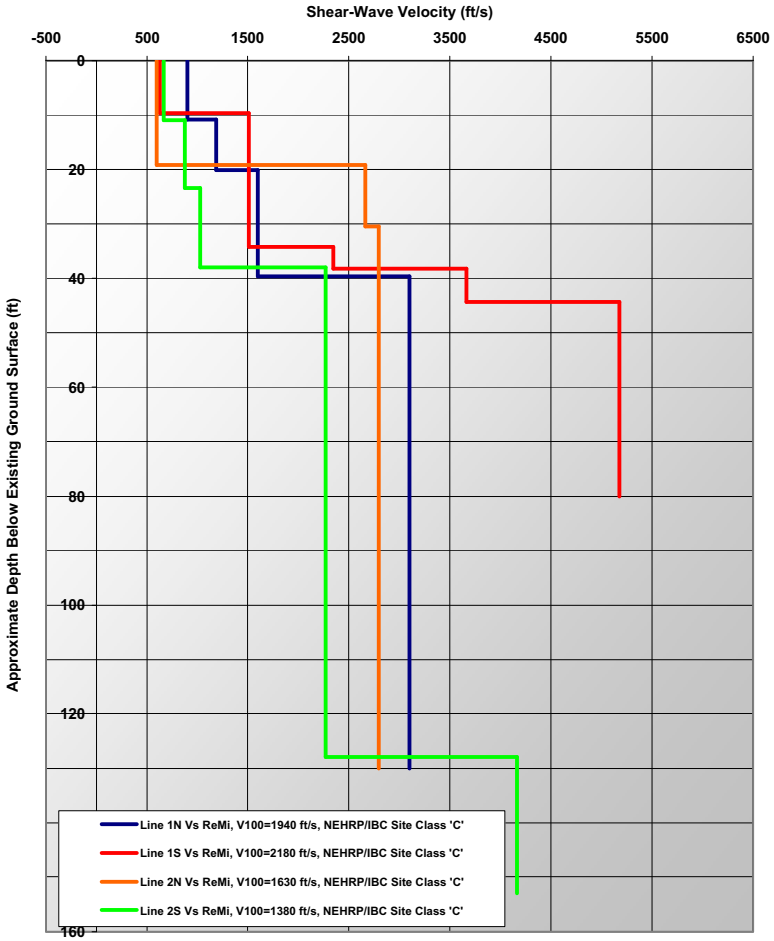

Fig. 3-4. Vertical ReMi soundings taken on Lines 1N, 1S, 2N, and 2S. Blue line (1N) and red line (1S) both show increases at depths of 35-40 ft, interpreted as the top of unweathered, “competent” Mancos Shale.

Our landslide interpretation is shown in Figs. 3-5 and 3-6. There is some ambiguity about the location of the landslide basal failure plane, because the top of “in-situ Mancos Shale” in borehole PZ-2 does not coincide with a steep increase in either P-wave or S-wave velocity. The implication is that the actual failure plane is down 10-15 ft within the Mancos Shale.

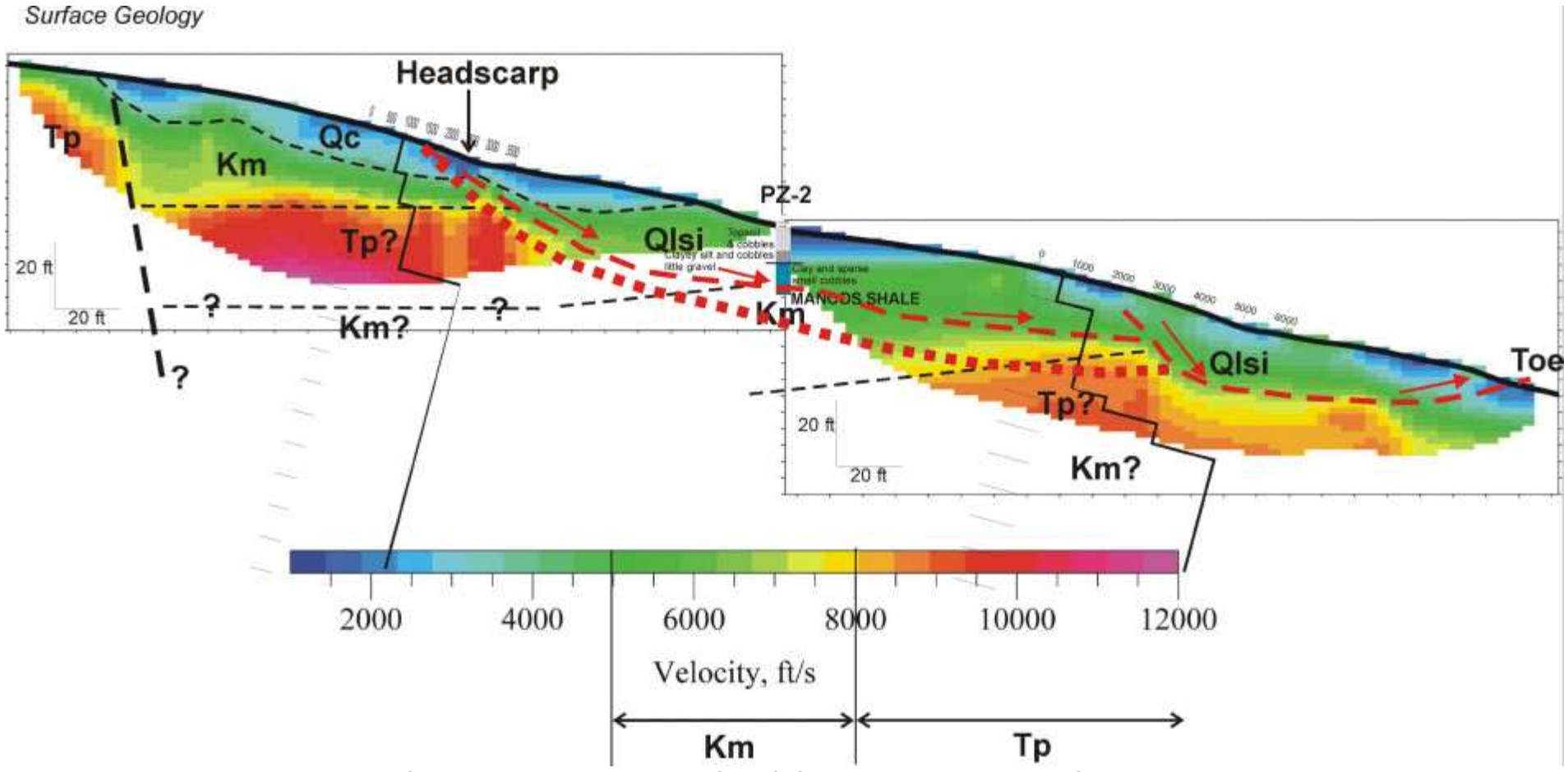

Fig. 3-5. Landslide interpretation of P-wave geophysics LINES 1N/1S and borehole PZ-2 at Snodgrass. Interpretation honors these observations: (1) apparent in-situ Mancos Shale in PZ-2 lies 20 ft below surface; (2) material is hard enough to cause rig refusal and is dry, unlike overlying softer deposits; (3) top of Mancos is about Vp=5000 fps; (4) these moderate velocities extend another 10-15 ft into Mancos before rising; (5) inferred Tp (Vp>10,000 fps) steps down-to-the-S twice, the larger step-down is ca. 60 ft; (6) velocity boundaries S of larger stepdown appear rotated into the hillslope, compared to those N of stepdown; (7) larger stepdown coincides with topographic headscarp and uphill limit of Qlsi interpreted from airphotos. Red dashed line shows interpreted slide plane that is forced to pass through top of bedrock exposed in borehole. Dotted red line shows a deeper possible slide plane that coincides with abrupt rise in S-wave velocities from ReMi.

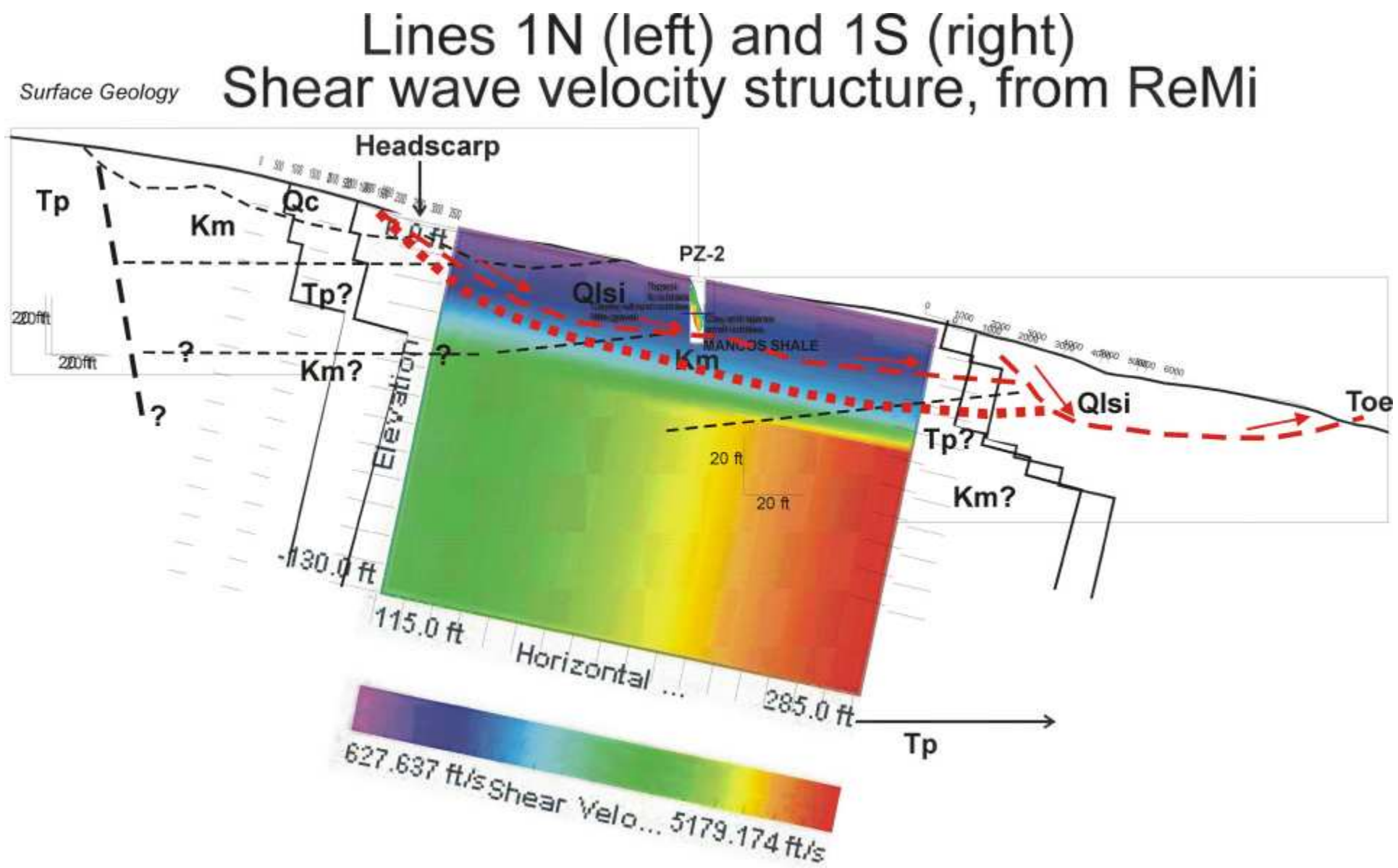

Fig. 3-6. Landslide interpretation of S-wave geophysics on LINES 1N/1S and borehole PZ-2 at Snodgrass. Interpretation places the landslide basal shear plane at the abrupt rise in S-wave velocities at depth of 35-40 ft. This is 15-20 ft deeper than where “in-situ Mancos Shale” was encountered in the borehole.

3.2.2 Lines 2N and 2S

Lines 2N and 2S cross the Ken's Crux landslide (polygon 22), a small Qlsy directly east of Ken's Crux (Figs. 3-5, 3-6). Line 2 is the northernmost line in a series of 5 contiguous spreads that extend a total of about 2400 ft downslope, lying under the main lift line up the SE slope of Snodgrass.

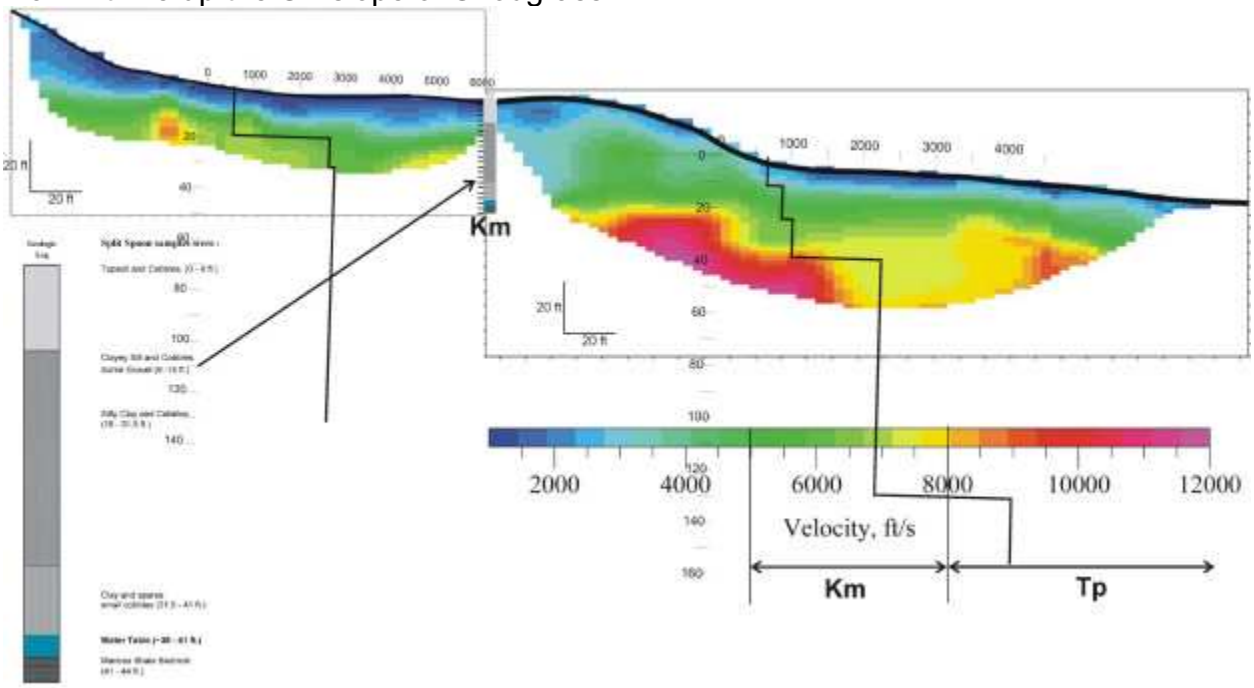

Fig. 3-5. P-wave tomogram, Lines 1N and 1S. The S-wave vertical profile from each line is superimposed.

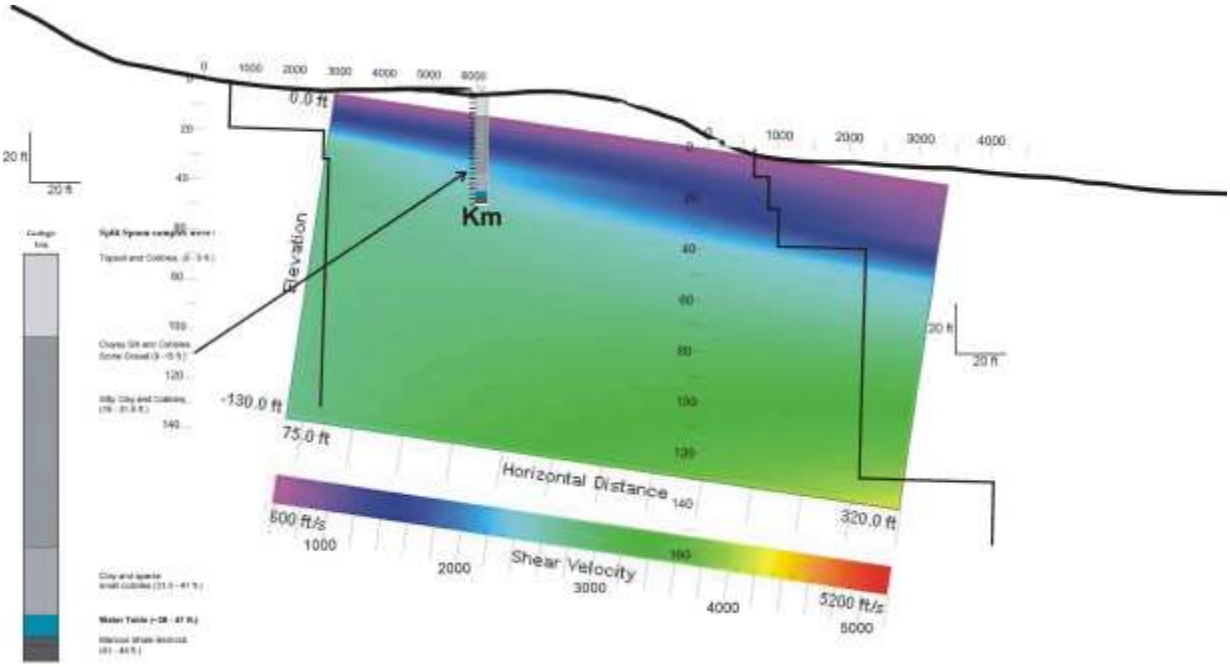

Fig. 3-6. Pseudo 2D S-wave tomogram based on the 2 vertical ReMi soundings.

The southern part of the line continues SE across an older Qlsi terrain. The uninterpreted P-wave tomogram is shown in Fig. 3-5 and a pseudo 2D ReMi tomogram is shown in Fig. 3-6, based on the vertical ReMi soundings shown in Fig. 3-4.

The Vs tomogram indicates relatively low velocities (dark blue, 1200-2000 fps; light blue, 2000-2600 fps) down to about 38 ft; this is where the water table lies. According to the well log, all this upper material is landslide debris. Below 38 ft the Vs values basically cease to increase down to 130 ft, lying in the range 3000 fps. According to the well log, this material is probably Mancos Shale. Below LINE 2S at a depth of 128 ft, Vs increases to 4163 fps, equivalent to Vp=ca. 12,490 fps. This is probably Tertiary porphyry.

On Line 2N, there is apparent contradiction between the Vs profile and Vp profile; Vs increases to 2661 fps at 19 ft (roughly equivalent to ca. 7983 fps Vp); in contrast, the Vp tomogram shows no abrupt increase in Vp at 19 ft, and shows Vp of 500-5500 fps. On Line 2S, in contrast, there is no contradiction between the Vs and Vp profiles; Vs increases to 2267 fps at 38 ft (roughly equivalent to ca. 6801 fps Vp); and the Vp tomogram shows an abrupt increase in Vp at about same depth, to about 8500 fps. We interpret this sharp increase as the top of in-situ Mancos Shale.

Therefore, our preferred shallow failure plane (Fig. 3-7) extends from the headscarp, down through the top of shale in borehole PZ-4, and continues southward at that same depth along the sharp velocity increase, finally rising to the base of the toe scarp. Notably, similar moderate-velocity (landslide?) material continues in the subsurface beyond the toescarp of polygon 22 (Fig. 3-8). This we interpret as the older landslide deposits (Qlsi) mapped SE of polygon 22.

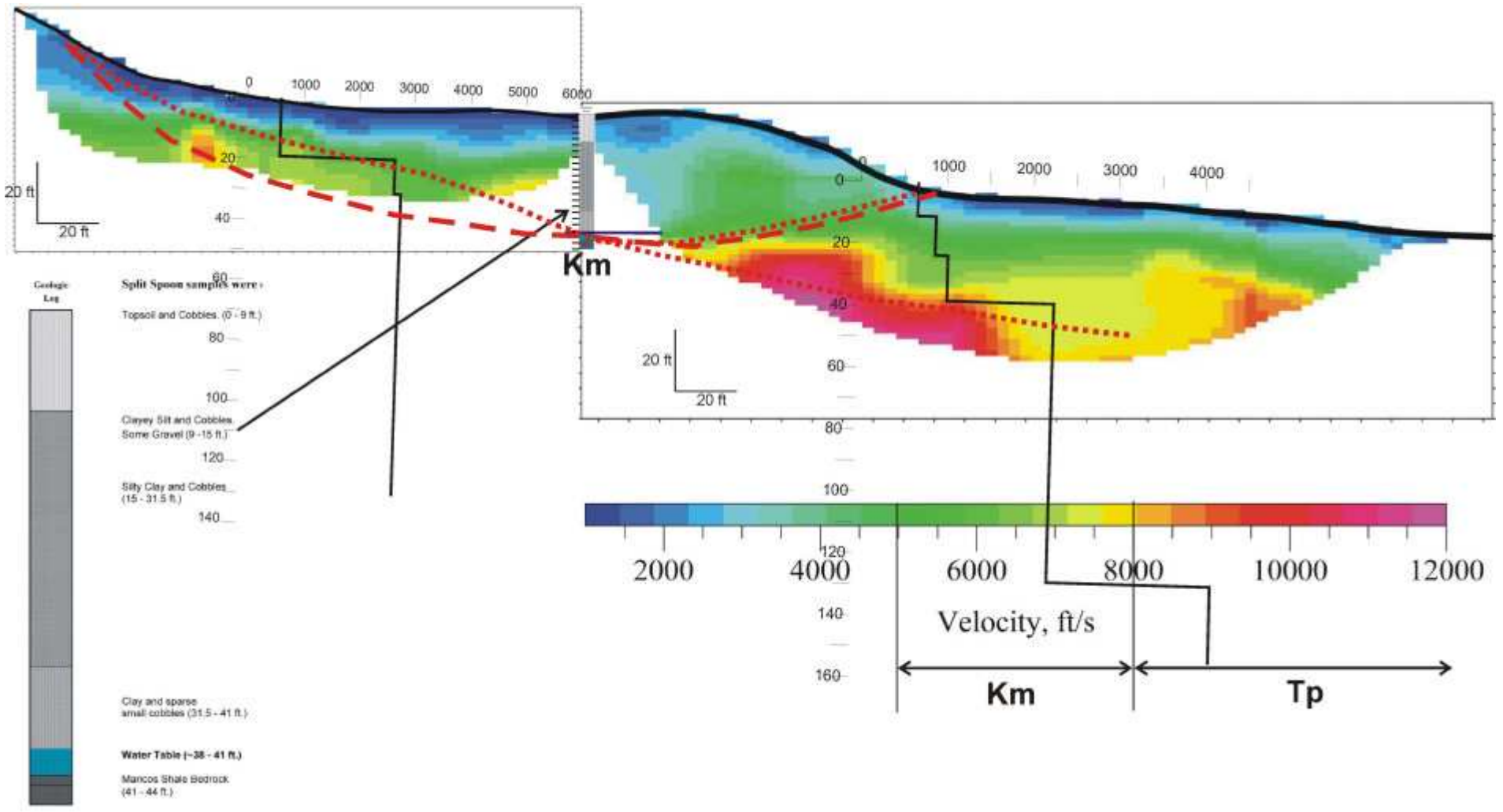

Fig. 3-7. Landslide interpretation of P-wave geophysics LINES 2N (left half) and 2S (right half), separated by borehole PZ-4 at Snodgrass. Interpretation honors these observations: (1) apparent in-situ Mancos Shale in PZ-2 lies 38 ft below surface; (2) material is hard enough to cause rig refusal and is dry, unlike overlying softer deposits; (3) top of Mancos is about ca Vp=10,000 fps; (4) inferred Tp (Vp>10,000 fps) underlies toe of polygon 22. Red dashed line shows interpreted slide plane that is forced to connect the headscarp, the top of bedrock in the borehole, and the toe of the toescarp. Dotted red line shows the level at which S-wave velocities increase.

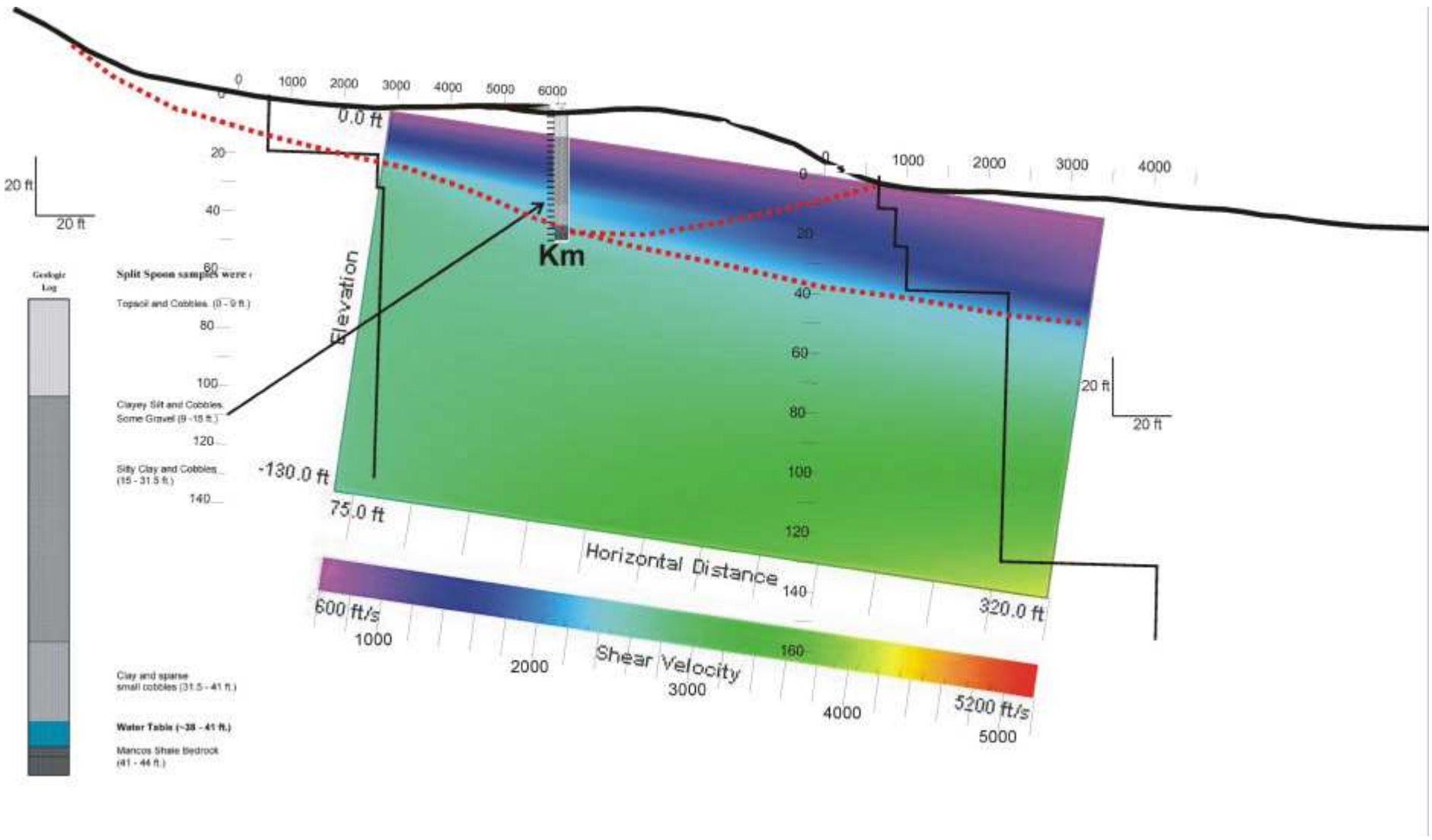

Fig. 3-8. Landslide interpretation of S-wave geophysics on LINES 2N/2S and borehole PZ-4 at Snodgrass. Interpretation places the top of undisturbed bedrock at the abrupt rise in S-wave velocities to >2500 ft/sec. This depth also corresponds with “in-situ Mancos Shale” encountered at -38 ft in the borehole.

3.2.3 Line 3

Line 3 continues downslope 480 ft SE from the SE end of Line 2S. It crosses the approximate center of the Middle Slide Complex (GHU 3) and landslide polygon 20, a small (8.4 acre) Qlsi downslope from Ken's Crux. The uninterpreted P-wave tomogram is shown in Fig. 3-9 and a pseudo 2D ReMi tomogram is shown in Fig. 3.9, based on the vertical ReMi soundings shown in Fig. 3.10. Interpretation of this line is deferred to Sec. 3.2.x, in which we interpret combined Lines 3-6.

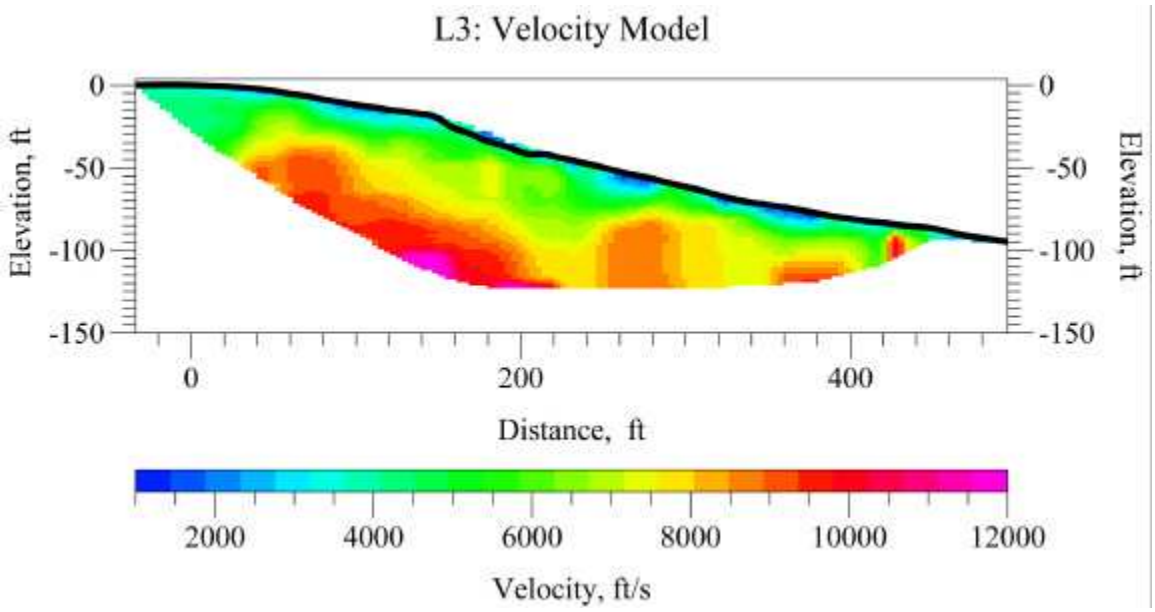

Fig. 3-9. P-wave tomogram, Line 3.

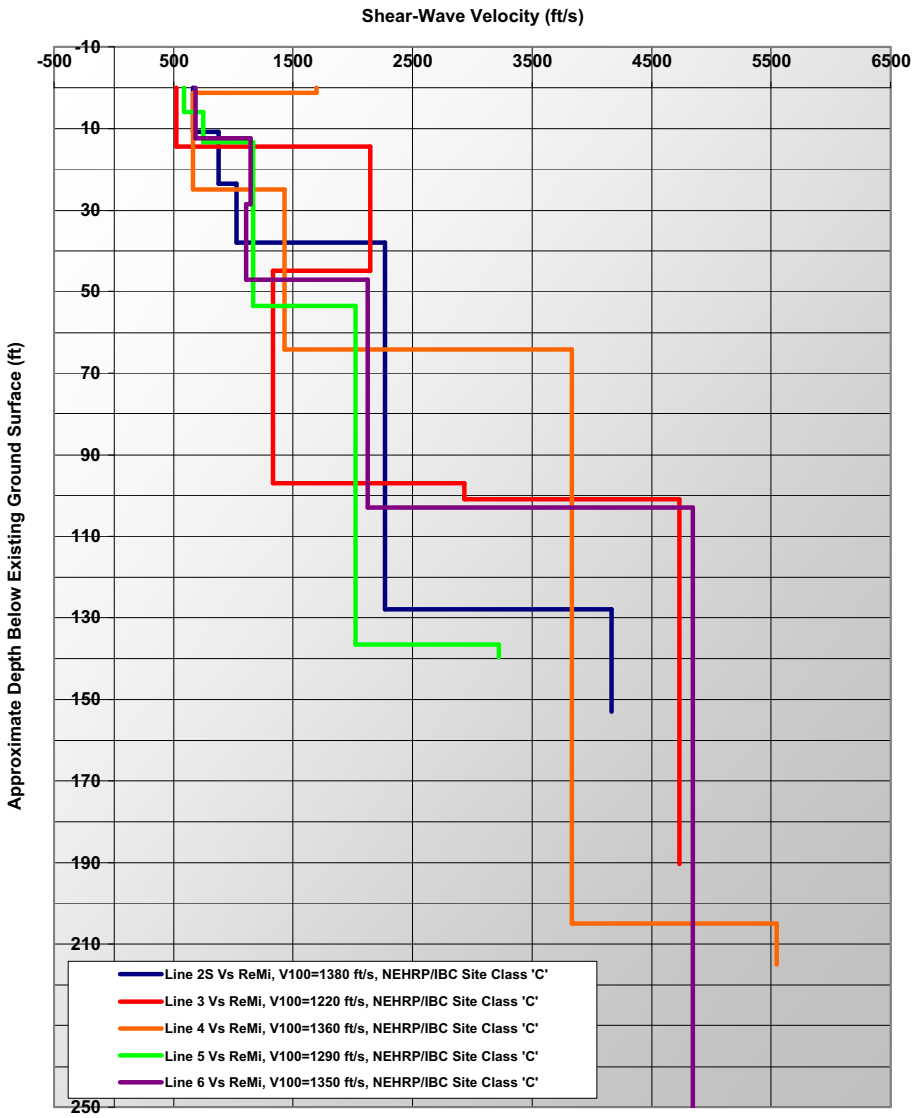

Fig. 3-10. Vertical ReMi soundings taken on Lines 2S, 3, 4, 5, and 6. Blue line (1N) and red line (1S) both show increases at depths of 35-40 ft, interpreted as the top of unweathered, “competent” Mancos Shale.

3.2.4 Line 4

Line 4 continues downslope 480 ft SE from the SE end of Line 3. It crosses the southern part of landslide polygon 20, the corner of polygon 23 (Qlsy), and the northern half of polygon 21 (Qlsiy). The uninterpreted P-wave tomogram is shown in Fig. 3-11. Interpretation of this line is deferred to Sec. 3.2.x, in which we interpret combined Lines 3-6.

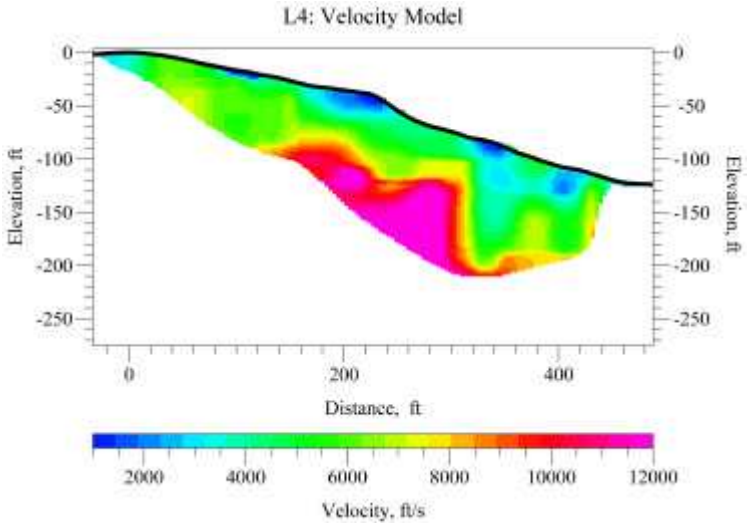

Fig. 3-11. P-wave tomogram, Line 4.

3.2.5 Line 5

Line 5 continues downslope 480 ft SE from the SE end of Line 4. It crosses the southern half of polygon 21 (Qlsiy), the toe of polygon 18 (Qlsi), and half of the Lower Earthflow (polygon 27, Qefo). The uninterpreted P-wave tomogram is shown in Fig. 3-12. Interpretation of this line is deferred to Sec. 3.2.x, in which we interpret combined Lines 3-6.

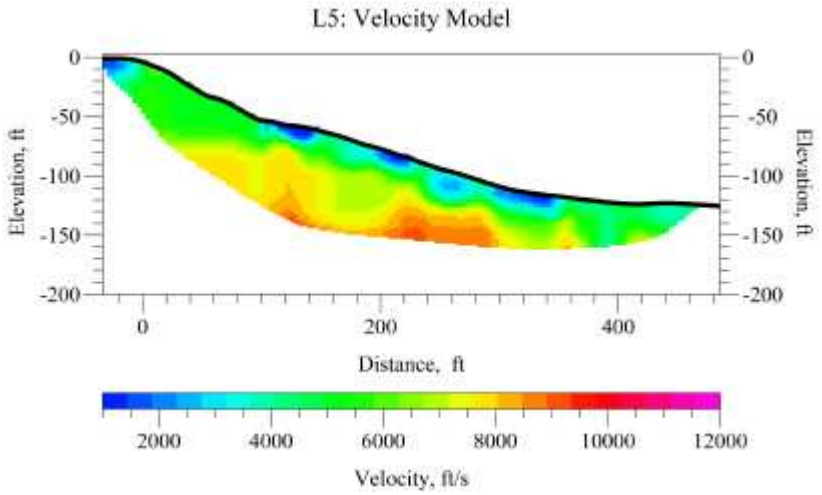

Fig. 3-12. P-wave tomogram, Line 5.

3.3 6 Line 6

Line 6 continues downslope 480 ft SE from the SE end of Line 5. It crosses the southern half of the Lower Earthflow (polygon 27, Qefo) and onto the Slump Block (polygon 16). The uninterpreted P-wave tomogram is shown in Fig. 3-13. Interpretation of this line is deferred to Sec. 3.2.x, in which we interpret combined Lines 3-6.

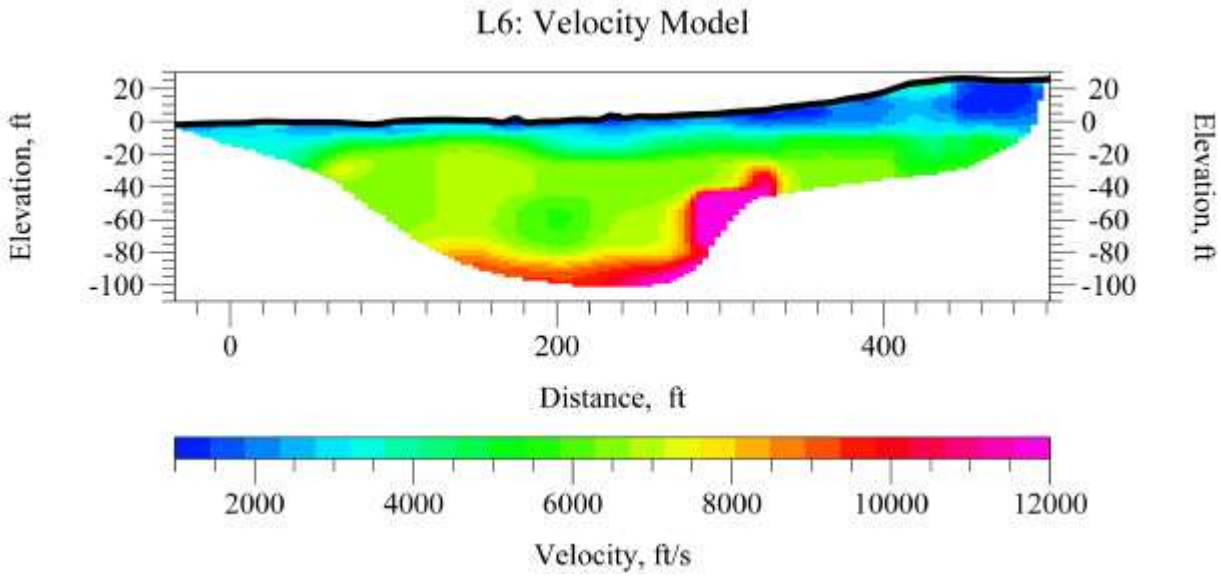

Fig. 3-13. P-wave tomogram of Line 6.

3.3.7 Combined Lines 3-6

To make interpretation easier, we mosaicked Lines 3 to 6 together to form a long transect. The geophysical interpretation of the component parts of the line has already been described above. The overall geologic-hydrologic interpretation of this long line, as well as other long lines, is found in Chapter 8.

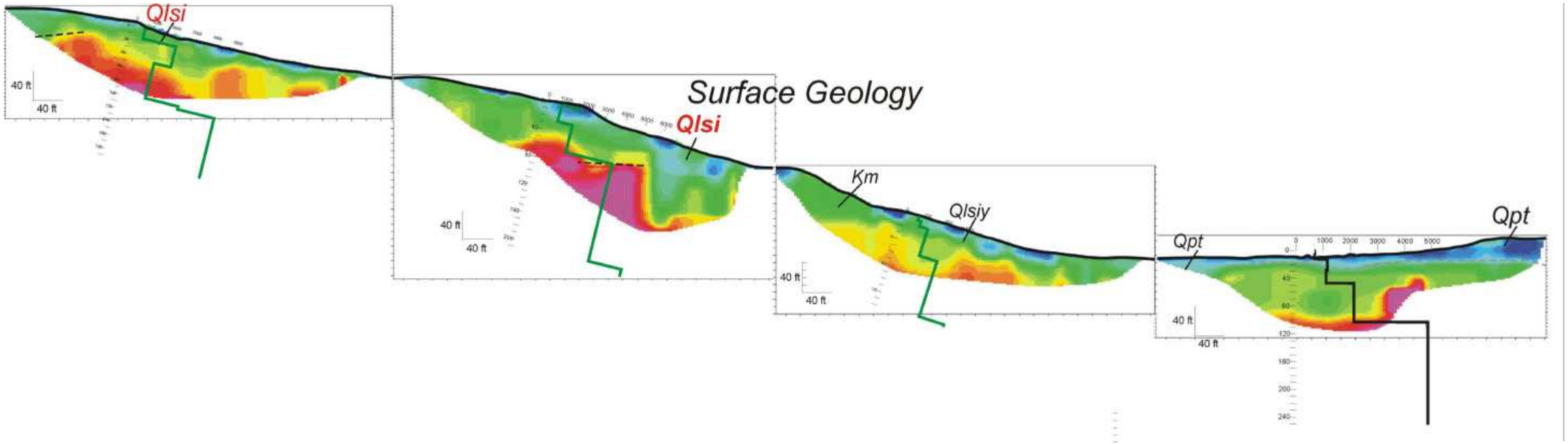

Fig. 3-14. Composite P-wave tomogram of Lines 3-6. ReMi shear wave soundings are shown as green or black lines in the center of each spread. Velocities faster than 11,000 ft/sec are assumed to represent Tertiary porphyry.

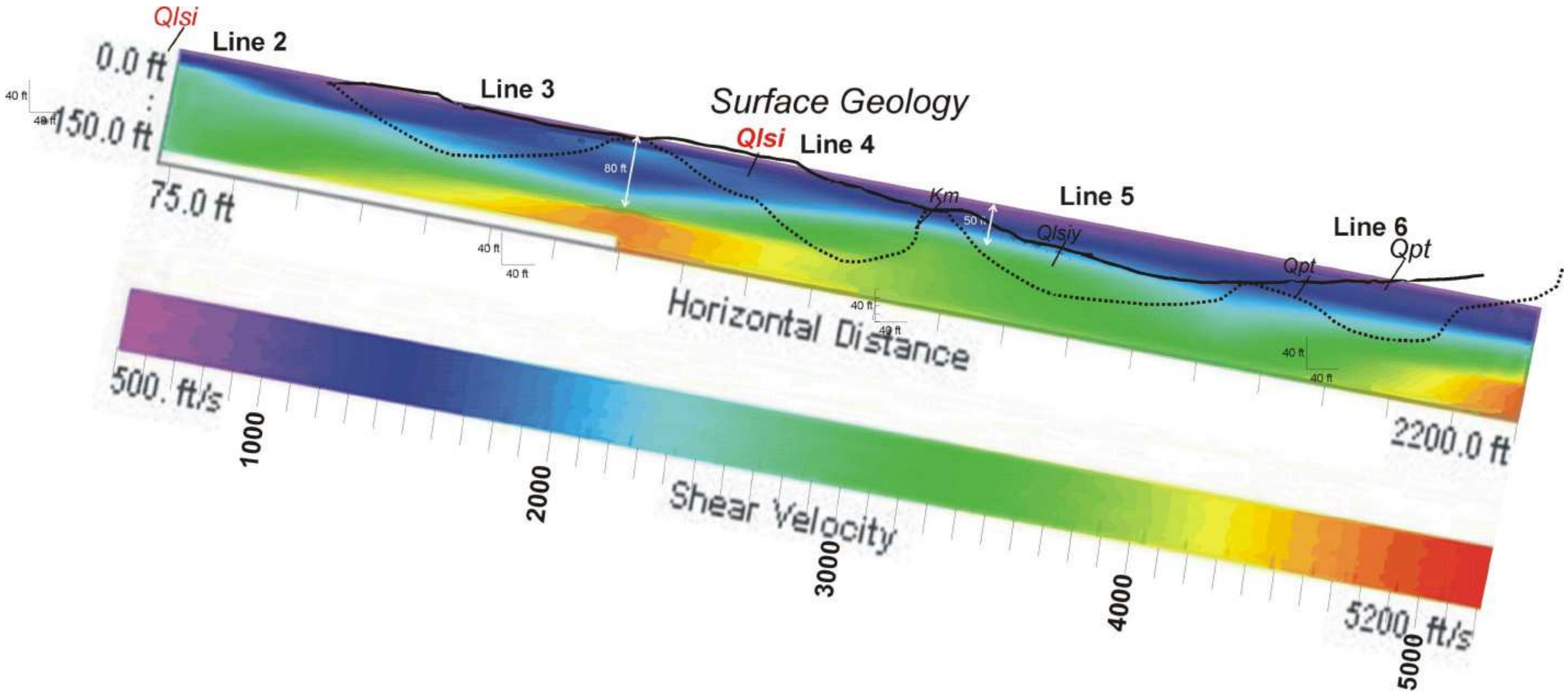

Fig. 3-15. Pseudo S-wave tomogram of Lines 3-6, made from ReMi shear wave soundings. Velocities faster than 4000 ft/sec are assumed to represent Tertiary porphyry.

3.4 Methods—Zonge Surveys of October 2007

This subchapter presents the results from the geophysical investigation conducted at the Proposed Crested Butte Mountain Resort Expansion site on the southeast side of Snodgrass Mountain, near Crested Butte, Colorado (see Fig.3-16). Twenty-eight 230-ft spreads of both compressional wave (P-wave) and shear wave (S-wave) refraction data were collected along three individual seismic lines, for an approximate total of 6,440 ft of P and S-wave refraction data coverage. The data were collected using a sledgehammer source at 11 and 9 shot points per spread for the P and S-wave data respectively. The furthest offset shot points were located 130 feet off either end of the spread, although 100 feet and 60 feet were predominantly used for the P and S-wave data respectively. The investigation, referred to as the Snodgrass Project herein, was conducted along three independent lines that were oriented parallel to the mountain side's slope as shown on Fig. 3-17. These three seismic lines are referred to as the West, Center and East Lines. Zonge Geosciences, Inc. (Zonge) performed the geophysical investigation under subcontract to GEOHAZ Consulting, Inc. (GEOHAZ). Field data were acquired from October 3rd through October 8th, 2007.

The start and end of each seismic line was selected by GEOHAZ personnel. The objectives of the geophysical investigation are fourfold: 1) to map the top of the Mancos Shale bedrock; 2) to determine thickness and lateral variability of unconsolidated landslide and glacial deposits; 3) to obtain P and S-wave velocities within these consolidated and unconsolidated materials; and 4) to identify the approximate distribution of fluid-saturated landslide deposits to help better constrain the location and geometry of failure planes at depth. These velocities may correlate with the mechanical strength and rippability of such materials. Furthermore, this information can be used to aid in the evaluation of subsurface conditions and associated geologic hazards relevant to the proposed Snodgrass Project. Based on the geologic setting and the site conditions outlined by GEOHAZ, Zonge determined a seismic survey approach using two-dimensional (2D) P-wave refraction and S-wave refraction tomography were selected to achieve the project objectives.

3.4.1 Site Description

The area of investigation includes three independent seismic lines located on the southeast side of Mt. Snodgrass. These seismic lines were generally oriented parallel to the mountain slope with the starts of the lines located on the uphill end. The site is approximately three miles due north of the town of Crested Butte, Colorado and just northwest of the Crested Butte Mountain Resort (CBMR) (see Fig.3-16). The seismic line start and ends were positioned and marked in the field by a GEOHAZ representative (see Fig. 3-17). The site exhibits porphyritic intrusive igneous rocks, landslide deposits consisting of Mancos shale and glacial deposits, and scarps (failure planes) exposed at the surface. Line locations were marked in the field using flagging on the ends of each 230-foot spread.

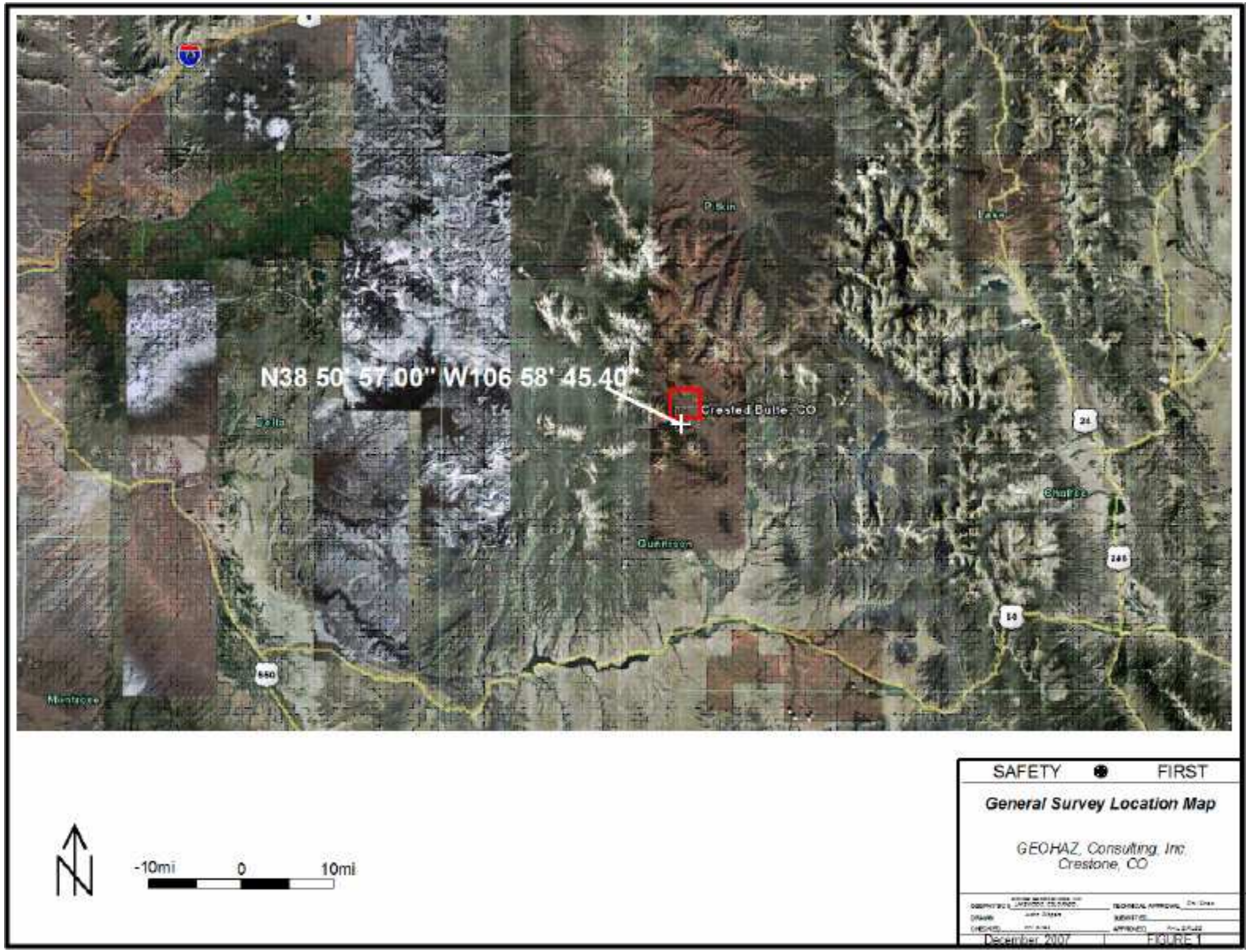

Figure 3-16 – Snodgrass location map (indicated by red box).

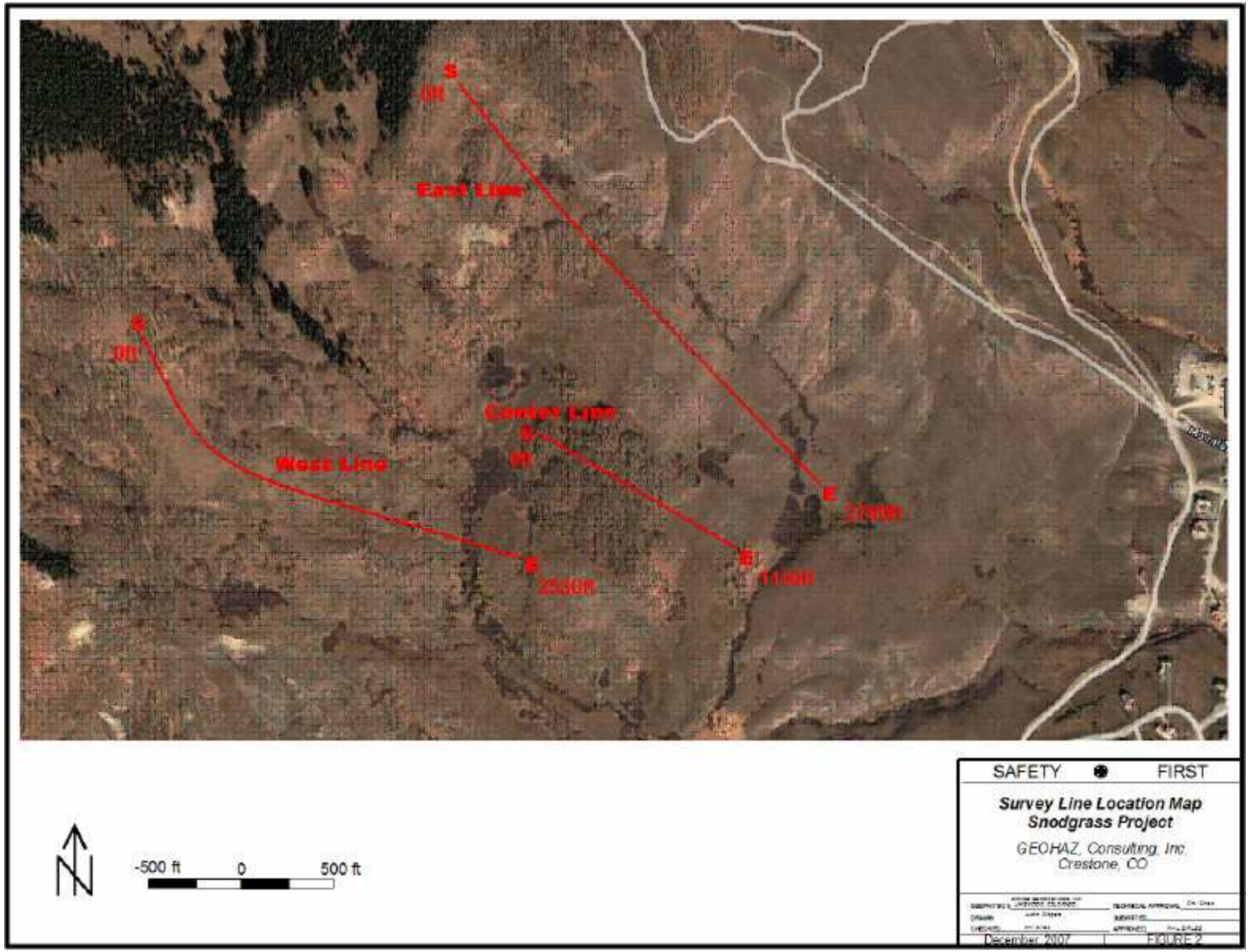

Fig. 3-17 – Snodgrass site map (seismic line locations indicated with red lines).

The immediate ground surface consisted of extremely soft soils and with light to thick vegetation. Lines were placed away from sources of cultural noise such as transmission lines, construction activities or traffic, however, intermittent windy conditions caused vibrational noise in areas where seismic sensors were near large aspen trees or shrubs. Care was taken in the timing of data collection to minimize the amount of noise in the data. Because wind was intermittent at the site, we were able to shoot between noise events, and this resulted in good to excellent data quality. Multiple hits per shot point were used to stack out the remaining vibrational noise from wind and flowing water in two small creeks crossed by during the survey.

3.4.2 Data Acquisition

Seismic refraction data were acquired at the Snodgrass site using a DAQ LinkII seismograph. This system utilizes a state of the art, 24-bit seismograph connected to a field laptop via ethernet cable. Analog data from the geophones are collected in the DAQ seismograph, anti-alias filtered, converted to a digital signal, transmitted to a laptop computer and recorded on the hard drive. DAQ modules have a 24-channel capacity, and one module was needed for this seismic investigation. Twenty-four P-wave or twenty-four S-wave receivers (geophones) were placed on the ground to form a given spread, and several spreads were required for each seismic line. The P-wave receivers were Mark Products, 4.5-Hz vertical component geophones, and the S-wave receivers were Oyo-Geospace 14-Hertz horizontal component geophones placed at the same receiver locations. P-wave receivers were placed vertically, and S-wave receivers were placed with the axis of sensitivity perpendicular to the seismic line.

Ten-foot geophone spacing was utilized for all lines resulting in 230 feet of data coverage for each spread. Line orientation was generally parallel with mountain slope (oriented up and downhill). Each of the three seismic lines consisted of several 24-channel spreads that were sequentially recorded and placed end-to-end in a roll-along manner for full data coverage along each seismic line. The start of each line was placed on the uphill end (to the northwest) resulting in tomograms, presented herein, being viewed as if the reader is “looking northeast.” Compressional-wave (P-wave) seismic energy was created with a 16-pound sledgehammer vertically striking an aluminum plate. Shear wave (S-wave) seismic energy was created with the same sledgehammer by striking both sides of a weight-coupled shear plate that was oriented perpendicular to each spread. 5 to 15 hammer blows at each shot point were used to transmit seismic energy across a given array of 24 geophones for both P-wave and S-wave refraction surveys (see inset picture below). The inset illustration shows the data acquisition geometry as used for each line at the Snodgrass site. Not shown are the ‘off-end’ shot points, which were located either 100 feet beyond each end of the spread(s) for the P-wave data and 60 feet beyond each end for the S-wave data. This setup results in a total of 11 P-wave shot points and 9 S-wave shot points per spread. Shot records were acquired for both shots performed on both sides of the shear plate. Shot records were acquired in SEG-2 format, using a 0.25 millisecond (msec) sample rate and 500 msec (½ second) record length.

Elevations at every source and receiver location were recorded using a hand level and stadia rod in the field. Calculated relative elevations were tied to borehole elevations and corrected to provide absolute elevations in feet. Observed elevations were consistently within a few inches of the measured elevations associated with the boreholes(see GEOHAZ borehole logs for elevations). Each seismic line crossed at least two boreholes to provide this elevation control.

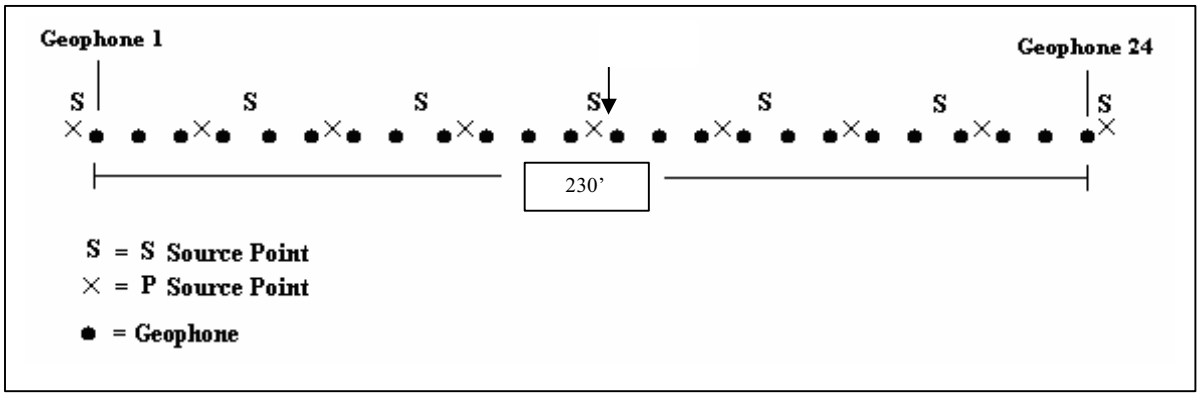

3.4.3 Data Processing

Refraction:

Refraction tomography is a modern extension of the seismic refraction method, and has been used to study the interior of the earth from scales of miles to tens of feet. The method was introduced in the 1980's, and uses a similar mathematical approach as the CAT scans (computed automated tomography) used for medical imaging. Tomography is the process of reconstructing spatial variations of a physical property (in this case seismic-wave velocity) from spatially distributed measurements that depend on that property (travel time). It follows that tomographic surveys require the measurement of travel times from large numbers of paths, or "ray-paths" through the media being imaged; in this case, soil and rock materials below the refraction spreads.

For this project the tomographic inversions were performed using a simulated annealing algorithm. First-break picks were made on all of the shot records acquired along each line. Travel times, along with source and receiver positions and elevations were formatted into files and input to the tomography software. Tomographic analysis was carried out using SeisOpt@2D™ (© Optim, Inc., 2006), a commercially available refraction tomography package produced by Optim, LLC (Version 4.0). A two-dimensional cross-section with velocity information at each subsurface point is produced. P and S-wave velocities can be correlated to the material type.

Simulated annealing is a Monte-Carlo estimation process that derives arrival times (P- and/or S-wave) and a velocity model from the data (Pullammanappallil and Louie, 1993; Pullammanappallil and Louie, 1994). The algorithm works by randomly perturbing an arbitrary starting model until the computed synthetic travel times match the travel times picked from the data with minimal error. Unlike linear, iterative inversions, simulated annealing optimization will find the global solution while avoiding

local error minimums. The method is insensitive to the starting velocity model, removing the interpreter bias. The fact that SeisOpt@2D makes no assumption about subsurface velocity gradients makes the method ideal for imaging laterally complex subsurface geology.

Refraction tomography allows reconstruction of both vertical and lateral velocity variations. The ray-path coverage for all rays traveling through the model is analyzed to determine coverage. A ray is a region in the model that has the highest contribution to the first arrival time. In this survey, the rays probed greater than 120 feet below the ground surface. The depth of investigation for any refraction survey is dependent on the receiver line length, and the velocity distribution of the subsurface materials, and the offset shot distance.

3.5 Results / Interpretations—Zonge Surveys of October 2007

Geologic and geotechnical borehole information have been provided by GEOHAZ for the area investigated using geophysics, and the seismic results have been correlated to these data in order to better constrain the interpretations based on seismic velocities calculated and presented here. Interpretations of the data are made based on the 2D P-wave and S-wave velocity distributions and gradients obtained by the tomographic results, geologic and borehole data and field observations.

The overburden soils are fairly uniform unconsolidated landslide deposits and glacial materials. According to data provided in borehole logs, these soils predominantly consist of silty and clayey sands, clays, Mancos shale fragments, gravels and larger clasts or boulders of decomposed porphyritic granite. Near the West Line, extremely weathered outcrops of the granites are exposed at the surface. These are either attached portions or blocks detached from sills of intrusive igneous materials present within the Mancos Shale and throughout the region. The intrusive materials are believed to originate from a batholith that uplifted and is located beneath Mt. Crested Butte. There are intervals of saturated soils and water indicated in the borehole logs as well.

3.5.1 Tomography

The 2D refraction results are presented as seismic sections (i.e., distance vs. elevation and velocity distribution) from the tomography analysis on Figs. 3-18 through 3-39. P-wave refraction results are presented in order for the West Line, followed by the Center Line and then the East Line on Figs. 3-18 through 3-28, and S-wave refraction results are presented in the same order on Figs. 3-29 through 3-39. Velocity scales are the same for all P-wave tomograms (0- 15,000 ft/s) and for all S-wave tomograms (300-7,000 ft/s). The elevation and distance scales are the same for all tomograms on a given figure, but they may vary slightly between figures due to varying depths of investigation on individual tomograms. Interpreted depth to weathered Mancos Shale is indicated on the tomograms with a dotted line.

The interpretation lines presented herein were based on the general trend and patterns of velocity distributions seen in the tomograms; the differences between the P and S-wave tomogram results for a given spread or location; the correlation between seismic velocities and the borehole data provided by GEOHAZ; and, field observations.

There is no set boundary or cut-off velocity for the top of the Mancos Shale, as expected in such a complex geologic setting, however, general trends in the tomograms match the borehole data very well, and interpolations can be made between boreholes with confidence. Question marks seen on the P and S-wave tomograms for the sixth spread along the West Line indicate that there is not adequate data to support an interpretation of top of weathered Mancos Shale in the vicinity of this location (see Figs. 19 and 30).

The velocities within the interpreted materials generally match those stated in a previous geotechnical report for a similar seismic investigation that was conducted on the same mountain slope. This unpublished report, entitled "Geophysical and Subsurface Investigations at the Proposed Mt. Crested Butte Municipal Reservoir Site," was presented to the Mt. Crested Butte Water & Sanitation District by Western Engineers, Inc. in 1986.

For actual depth to bedrock, the boring logs should be consulted (Appendix 6-1). The interpreted depth to weathered Mancos Shale places the material interface on the tomograms at an average P-wave velocity of about 7,500 ft/s and an average S-wave velocity of about 3,500 ft/s. These values are reasonable for fractured and weathered shale. These are the approximate average velocities shown on the tomograms along the location of the interpreted interface. Also, the interpretations presented here are further supported by patterns in the P-wave and S-wave velocity distributions and gradients that suggest an obvious change in material properties.

Interpretation of the P-wave refraction velocity sections obtained indicate two major velocity layers: low-velocity materials interpreted as unsaturated or saturated, unconsolidated landslide and glacial deposits (i.e., 1,000-7,500 ft/s P-wave velocities and 300-3,500 ft/s S-wave velocities), generally shaded in blue and green or "*cool*" colors, and; high-velocity materials (i.e.,>7,500 ft/sec P-wave velocities and > 3,500 ft/s S-wave velocities) interpreted as weathered or competent Mancos Shale, generally shaded in yellow and red or "*hot*" colors.

P-wave propagation velocities are dominated by a soil skeleton up to approximately 99.5% water saturation at which point the propagation velocity becomes dominated by the compressible pore-space fluid. At and above this saturation level, P-wave velocities jump up to approximately 4,900-5,100 ft/s, and this makes it difficult to distinguish between weathered rock and saturated soils based solely on P-wave velocities calculated by refraction techniques. In regions believed or known to contain saturated soils, the differences in trends of P-wave and S-wave velocity distributions can help to determine the actual depth to rock and avoid skewed interpretations due to increased P-wave velocities within saturated and unconsolidated materials. Examples of this difference in velocity distribution trends can be seen on the tenth spread along the West Line and on the fifth spread along the East Line (see Figs. 3-21 and 3-32 for the West Line and Figs. 3-25 and 3-36 for the East Line). At these two locations, standing or flowing water observed in the field suggests the presence of saturated soils near the surface, and the interpreted depth to Mancos Shale becomes more dependent on the distributions of S-wave velocities at depth. In general, the possibility of saturated soils existing near the surface increases in regions where the P-wave tomograms have a sudden increase to velocities of about 4,900 ft/s or greater while the complimentary S-wave tomograms show consistently low velocities in the same vicinity.

Five observations provide confidence in the geophysical results:
1) The seismic data quality ranged from good to excellent; **2)** Alternate processing methods produced consistent results; **3)** There is good correlation between seismic results and field observations; **4)** There is excellent correlation between the P-wave and S-wave tomographic solutions, and; **5)** There is good correlation between seismic models and borehole data provided by GEOHAZ.

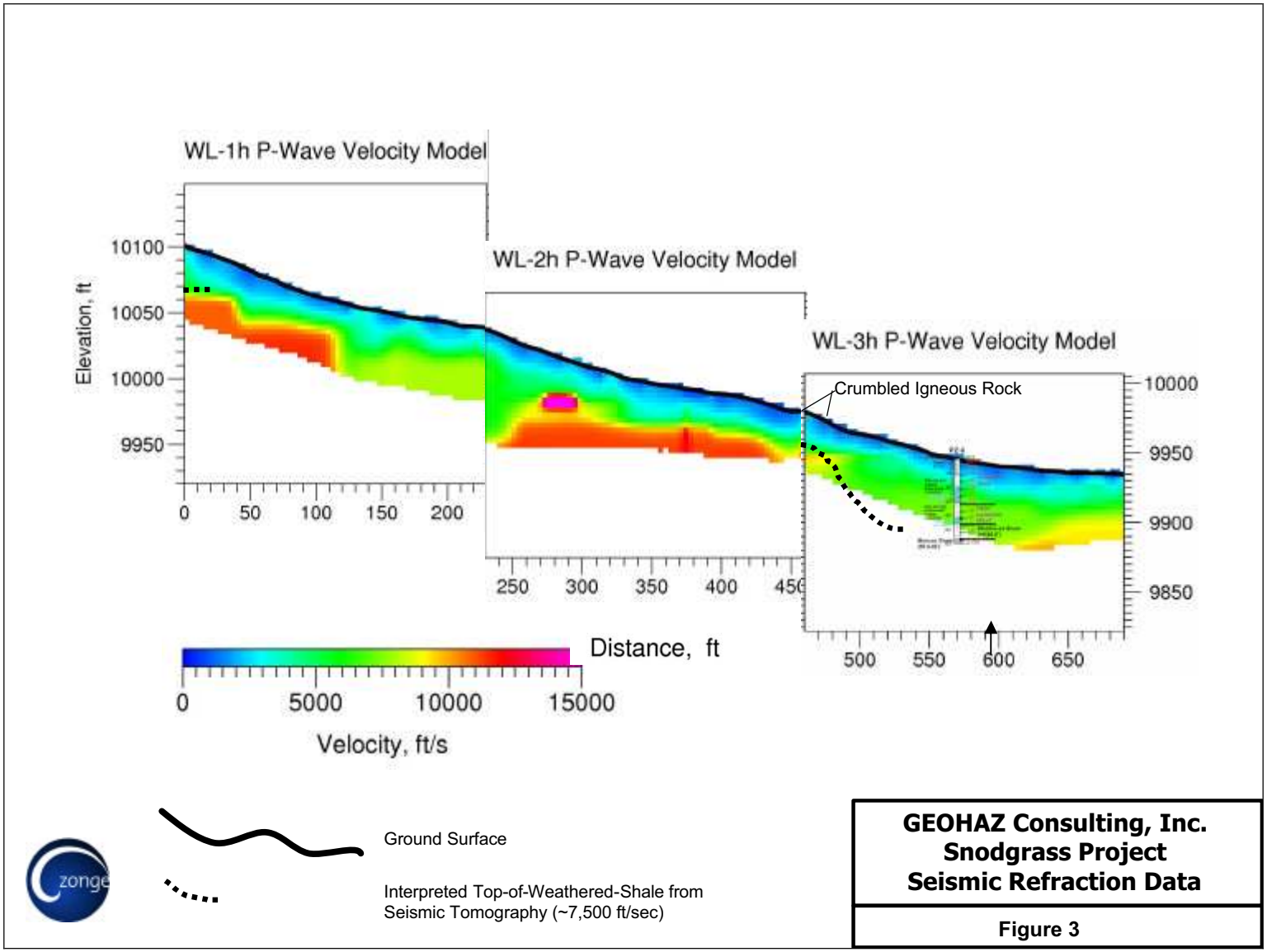

Figure 3-18. Snodgrass, WL-1, 2, 3 P-wave refraction tomograms.

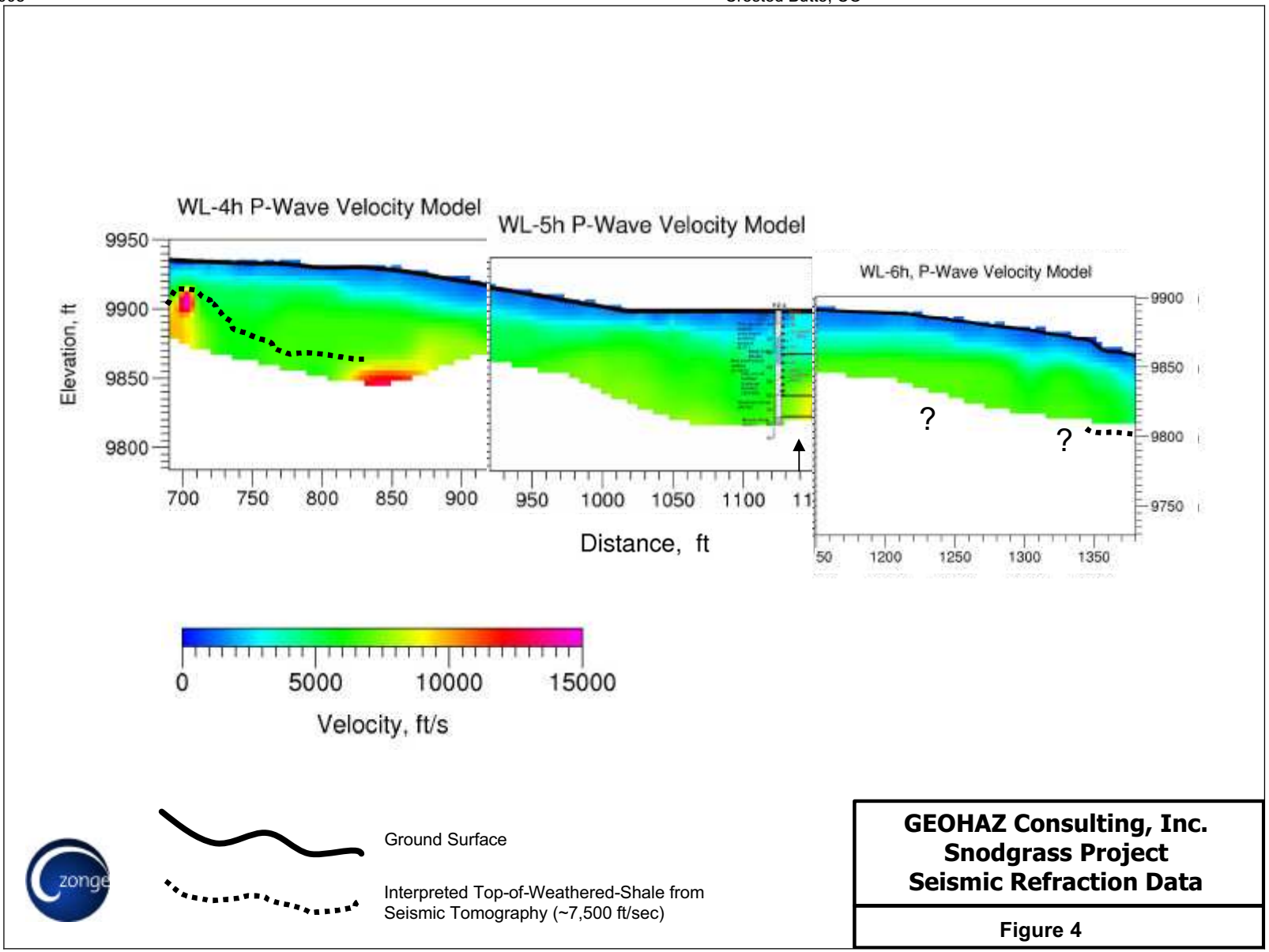

Fig. 3-19. Snodgrass, WL-4, 5, 6 P-wave refraction tomograms

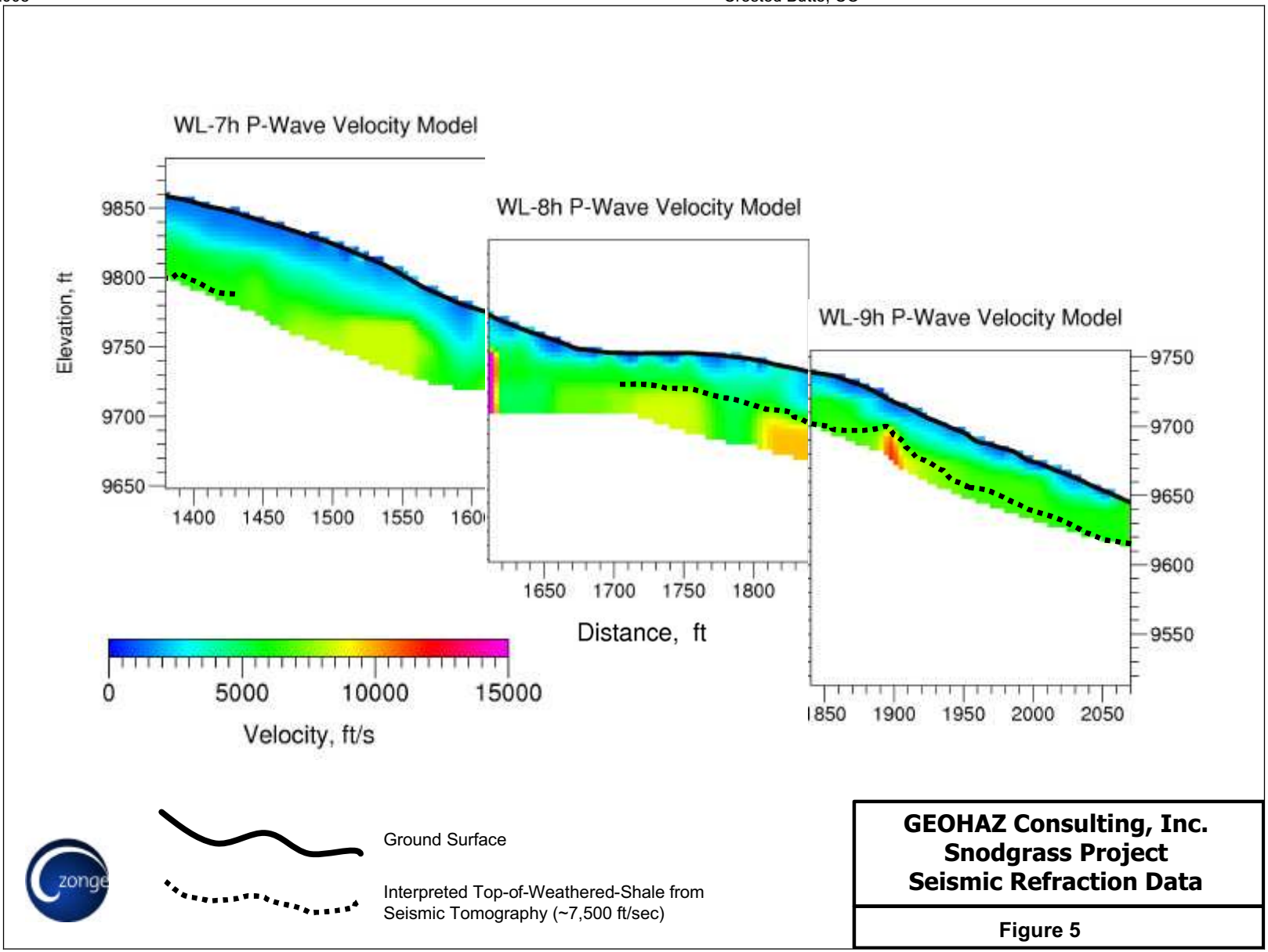

Fig. 3-20. Snodgrass, WL-7, 8, 9 P-wave refraction tomograms

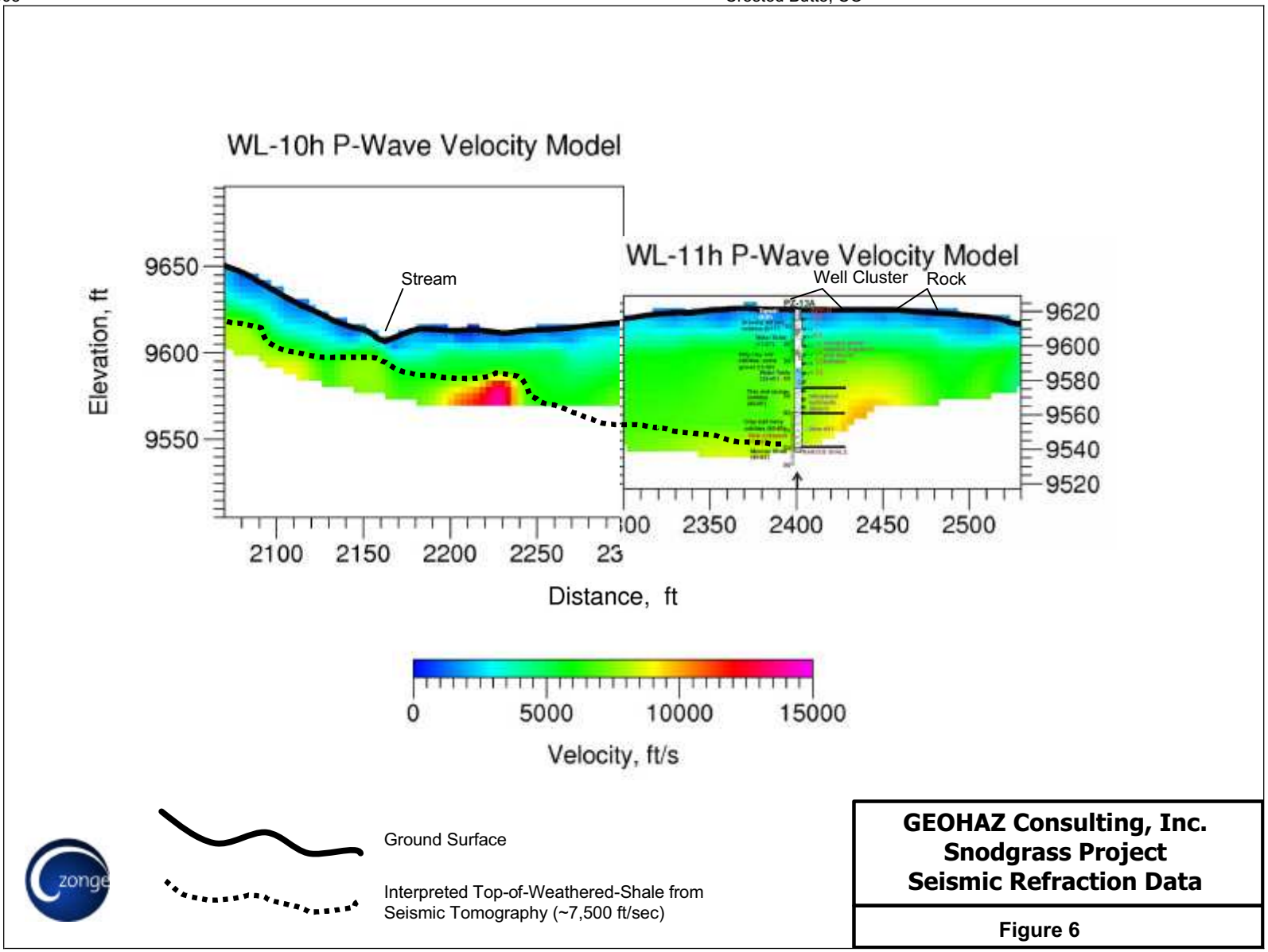

Fig. 3-21. Snodgrass, WL-10, 11 P-wave refraction tomograms

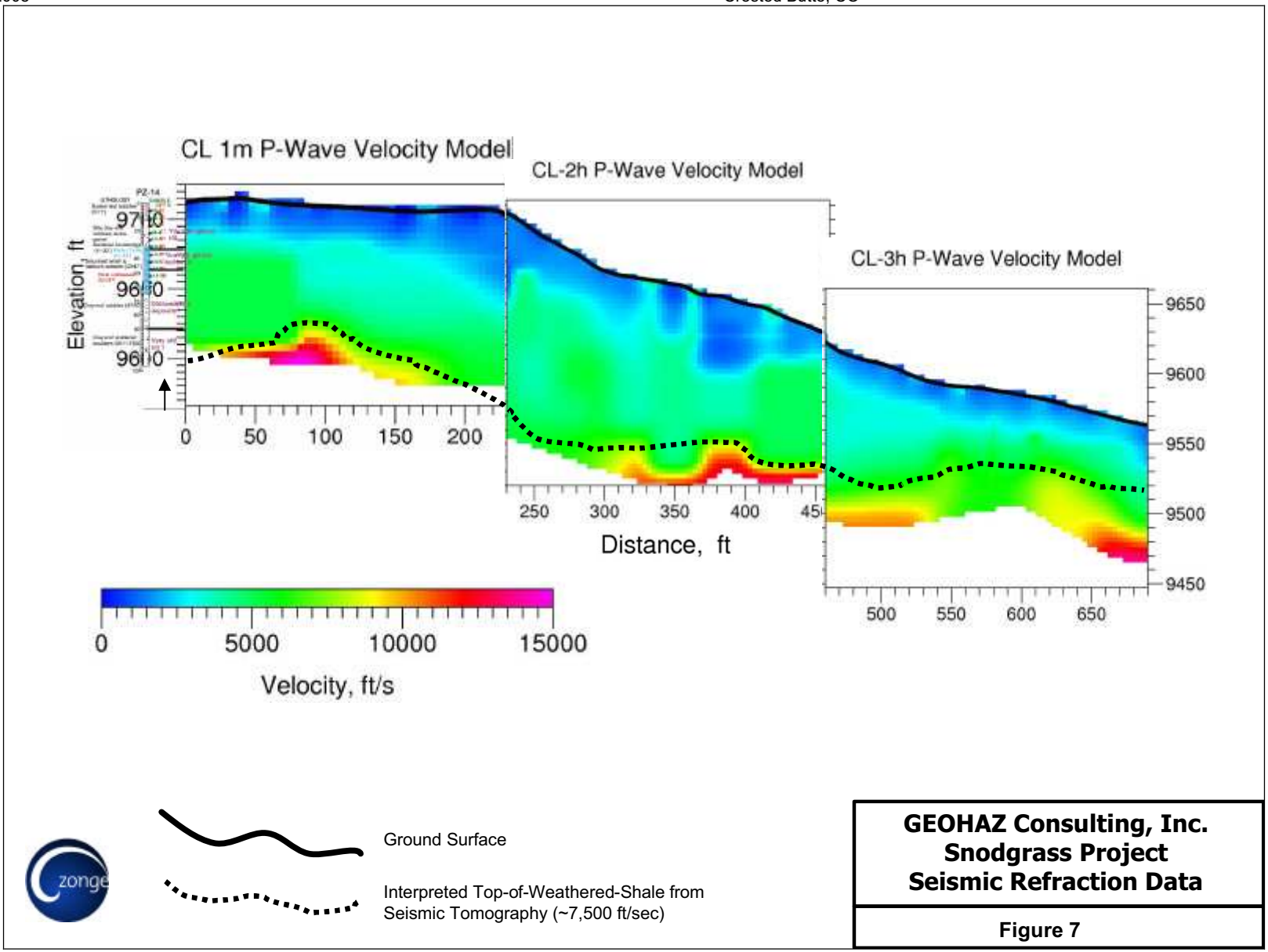

Fig. 3-22. Snodgrass, CL-1, 2, 3 P-wave refraction tomograms

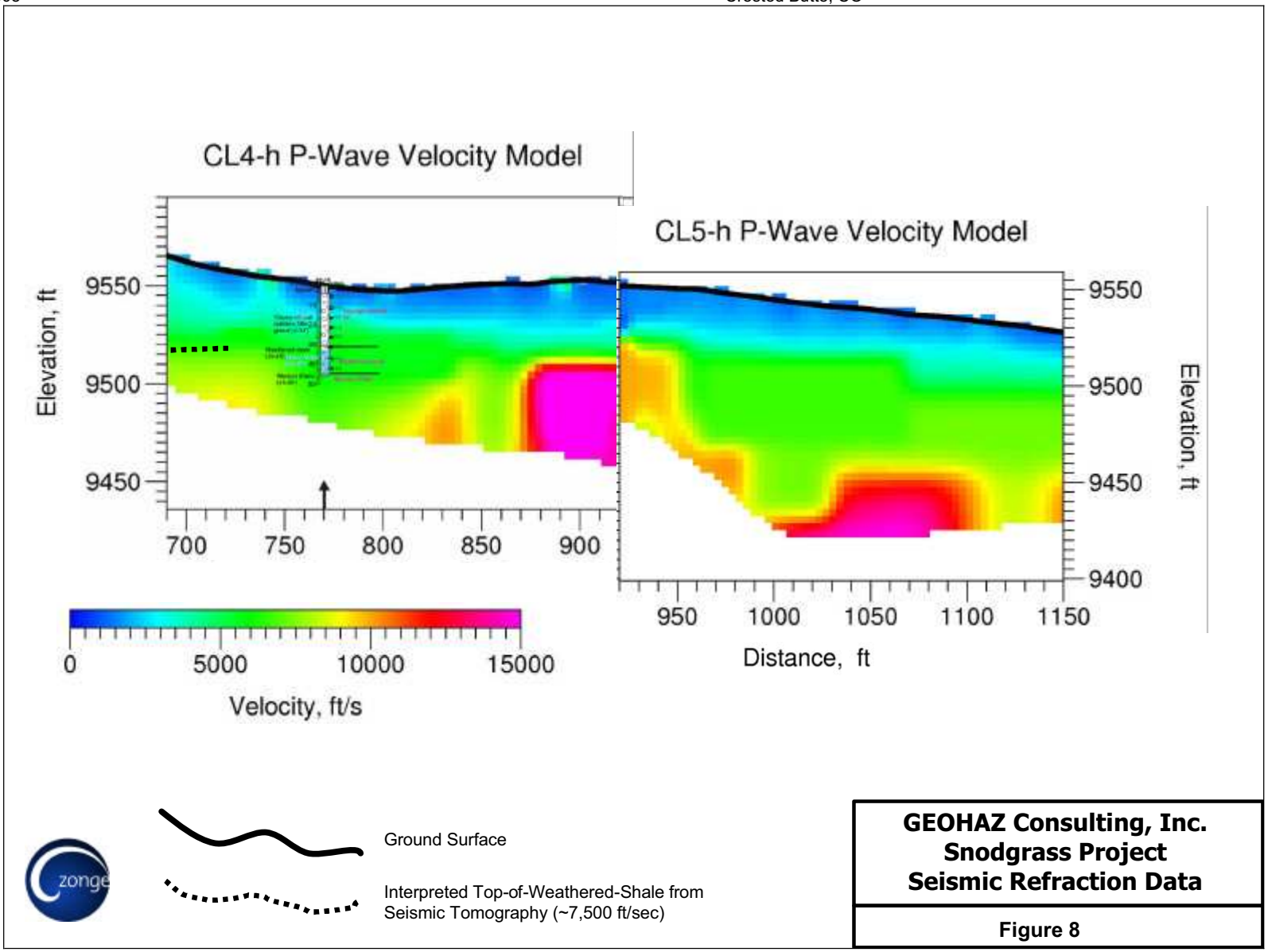

Fig. 3-23. Snodgrass, CL-4, 5 P-wave refraction tomograms

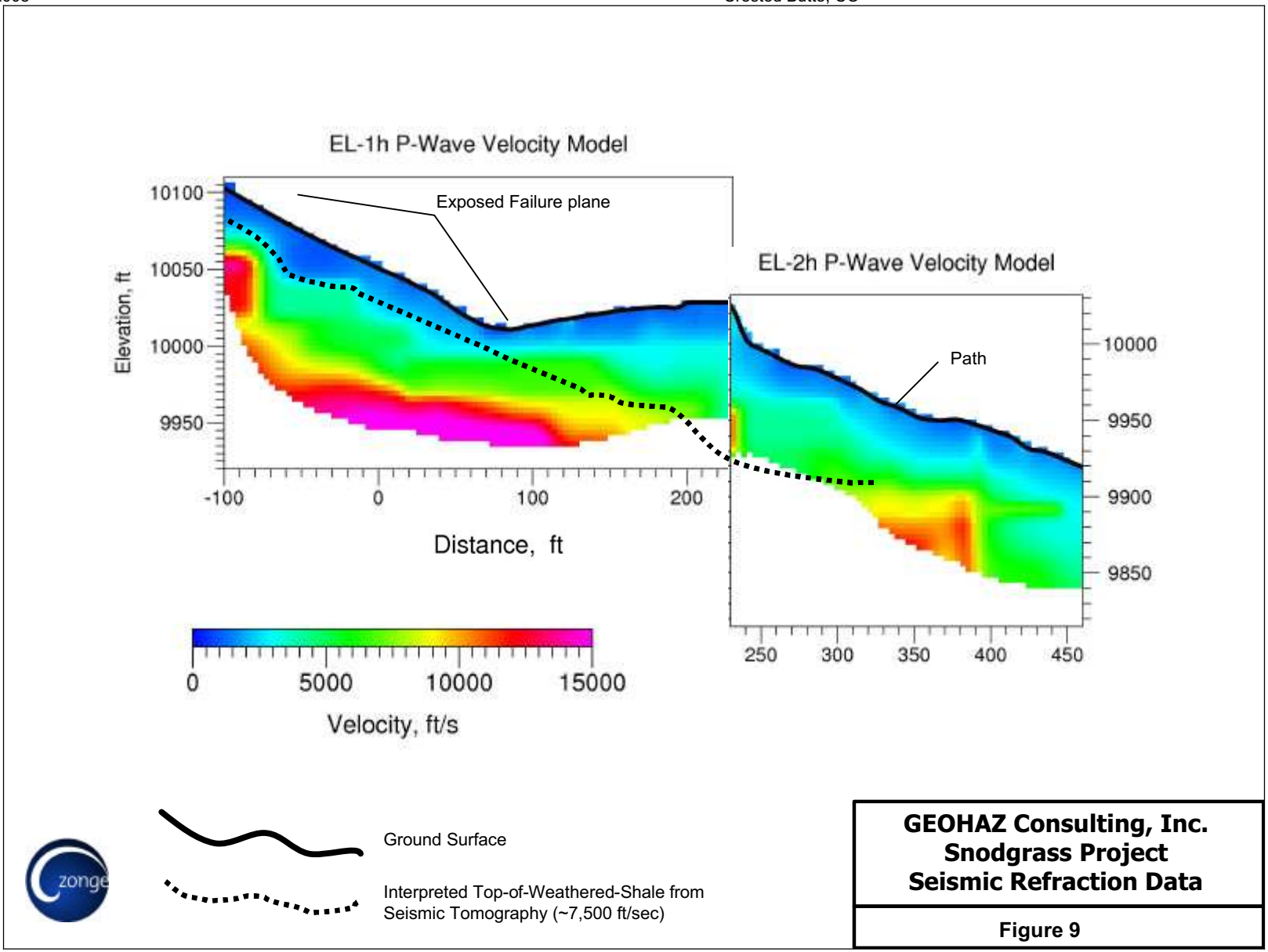

Fig. 3-24. Snodgrass, EL-1, 2 P-wave refraction tomograms

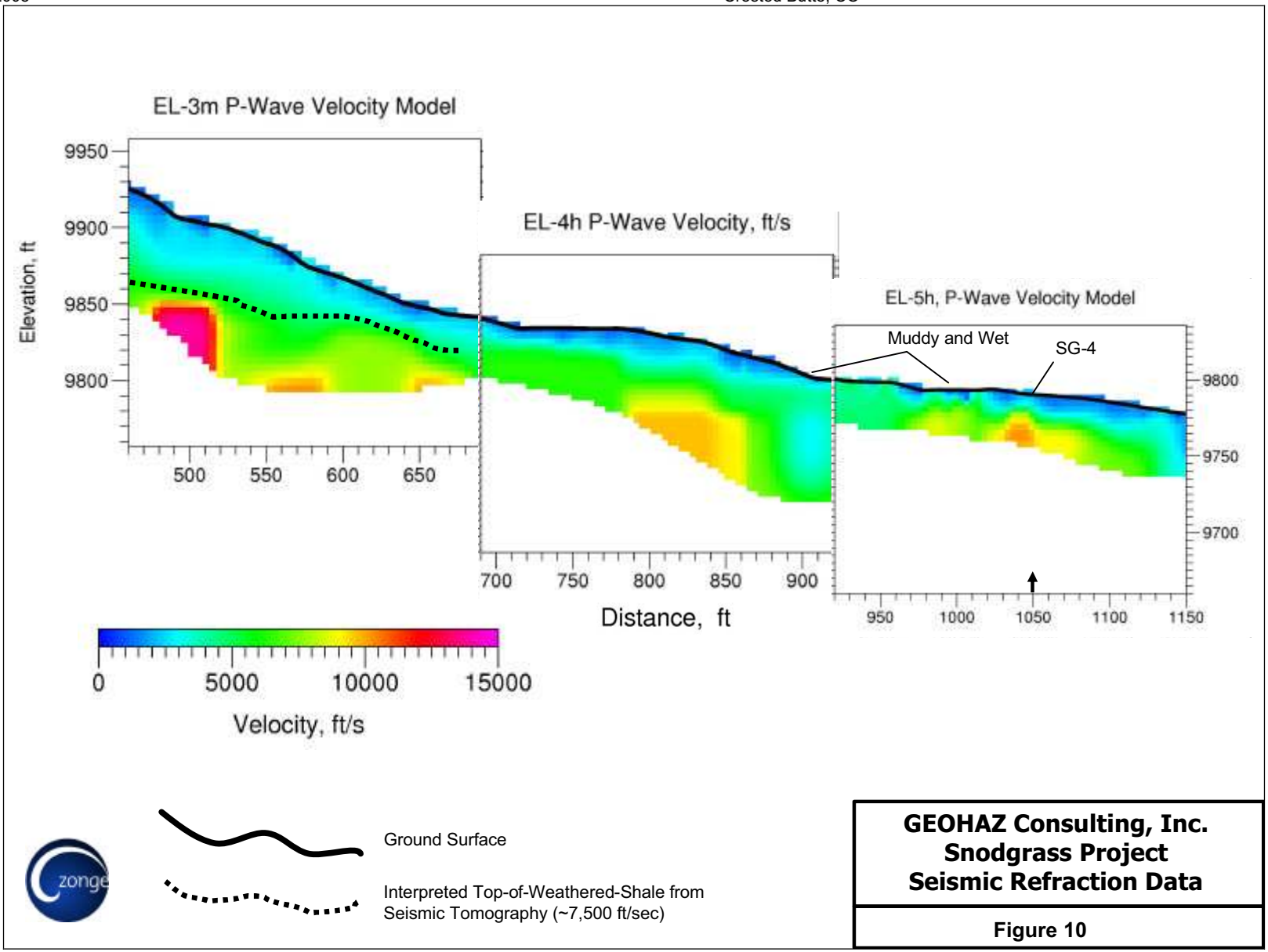

Fig. 3-25. Snodgrass, EL-3, 4, 5 P-wave refraction tomograms

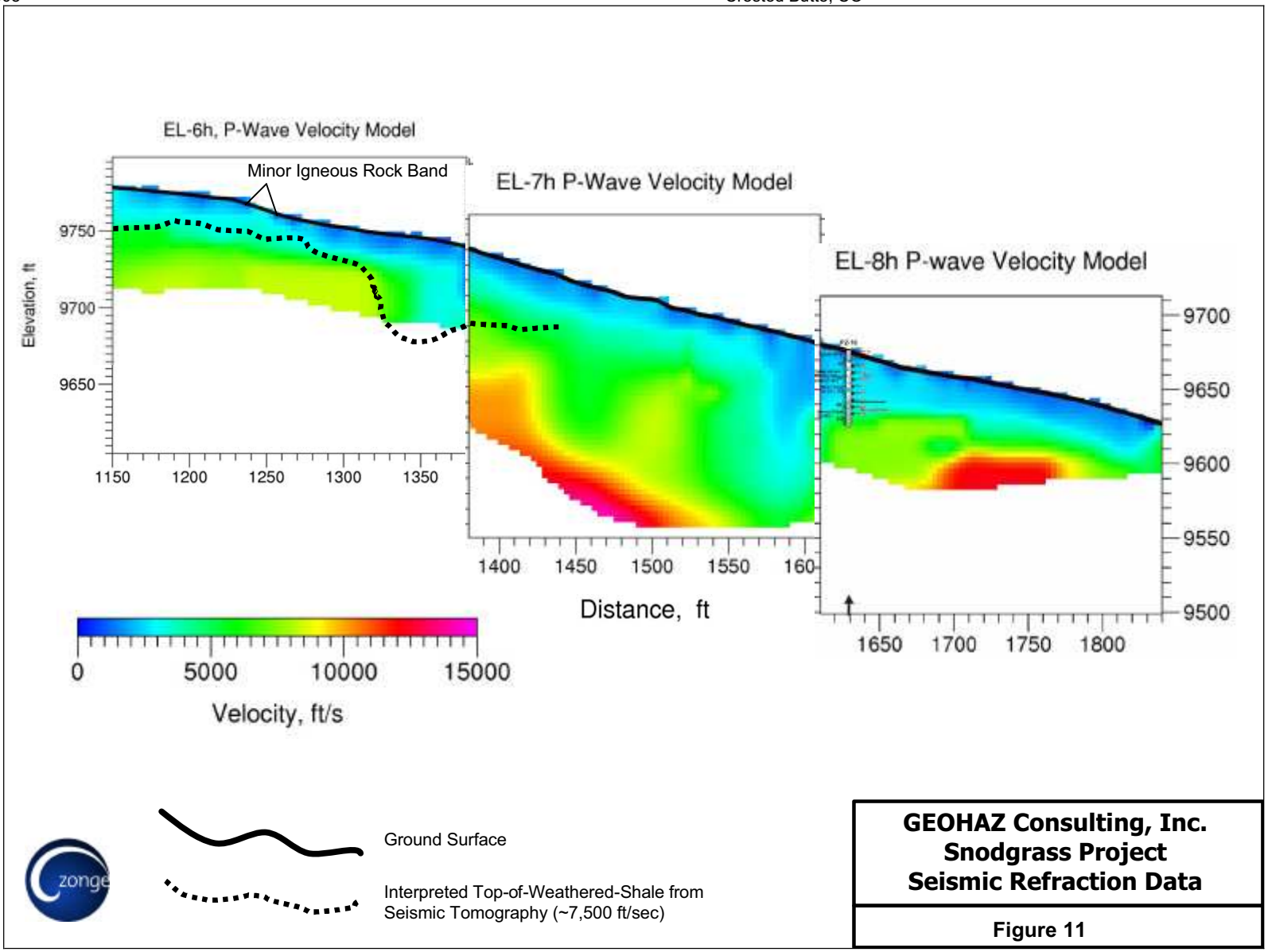

Fig. 3-26. Snodgrass, EL-6, 7, 8 P-wave refraction tomograms

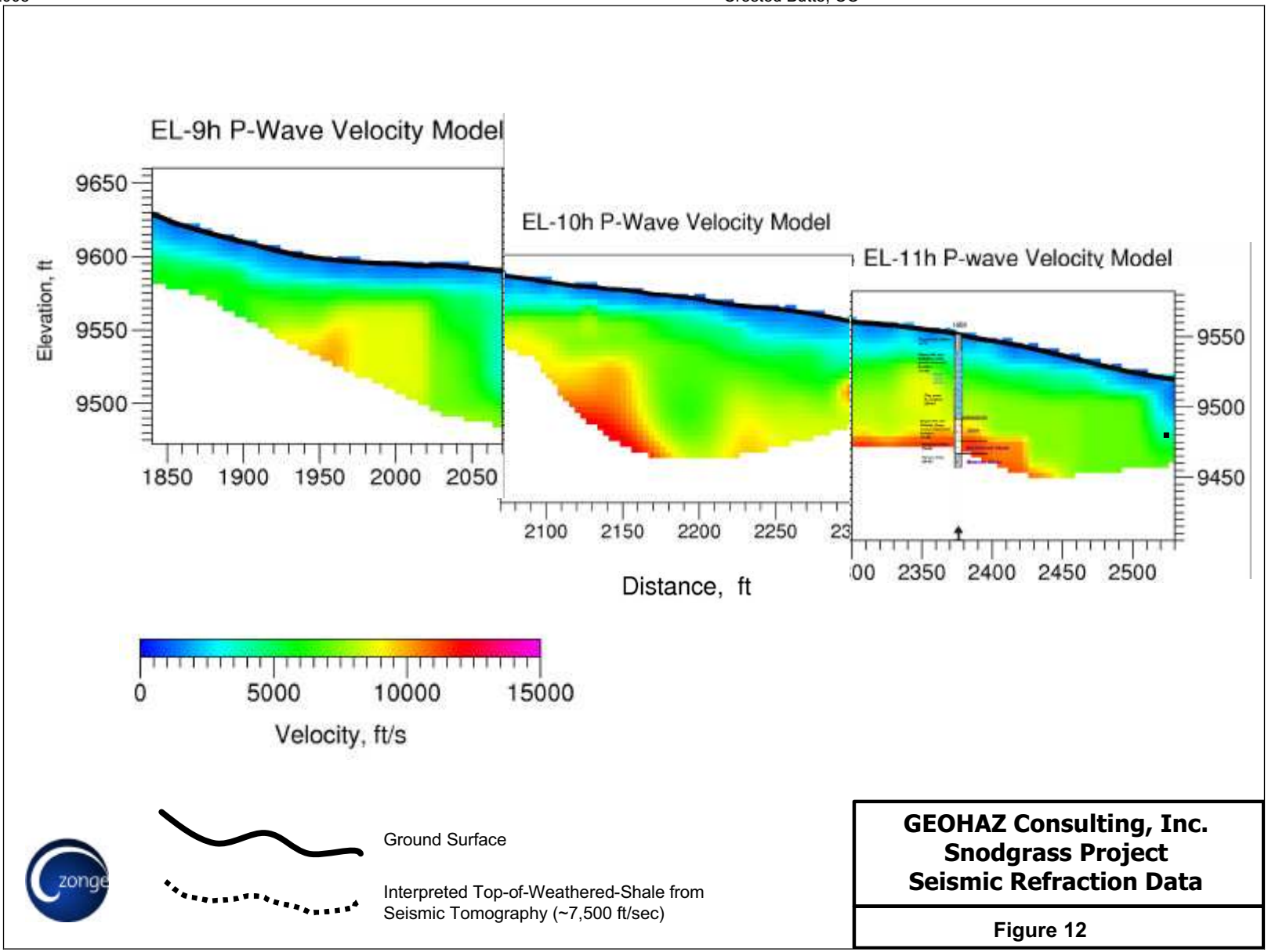

Fig. 3-27. Snodgrass, EL-9, 10, 11 P-wave refraction tomograms

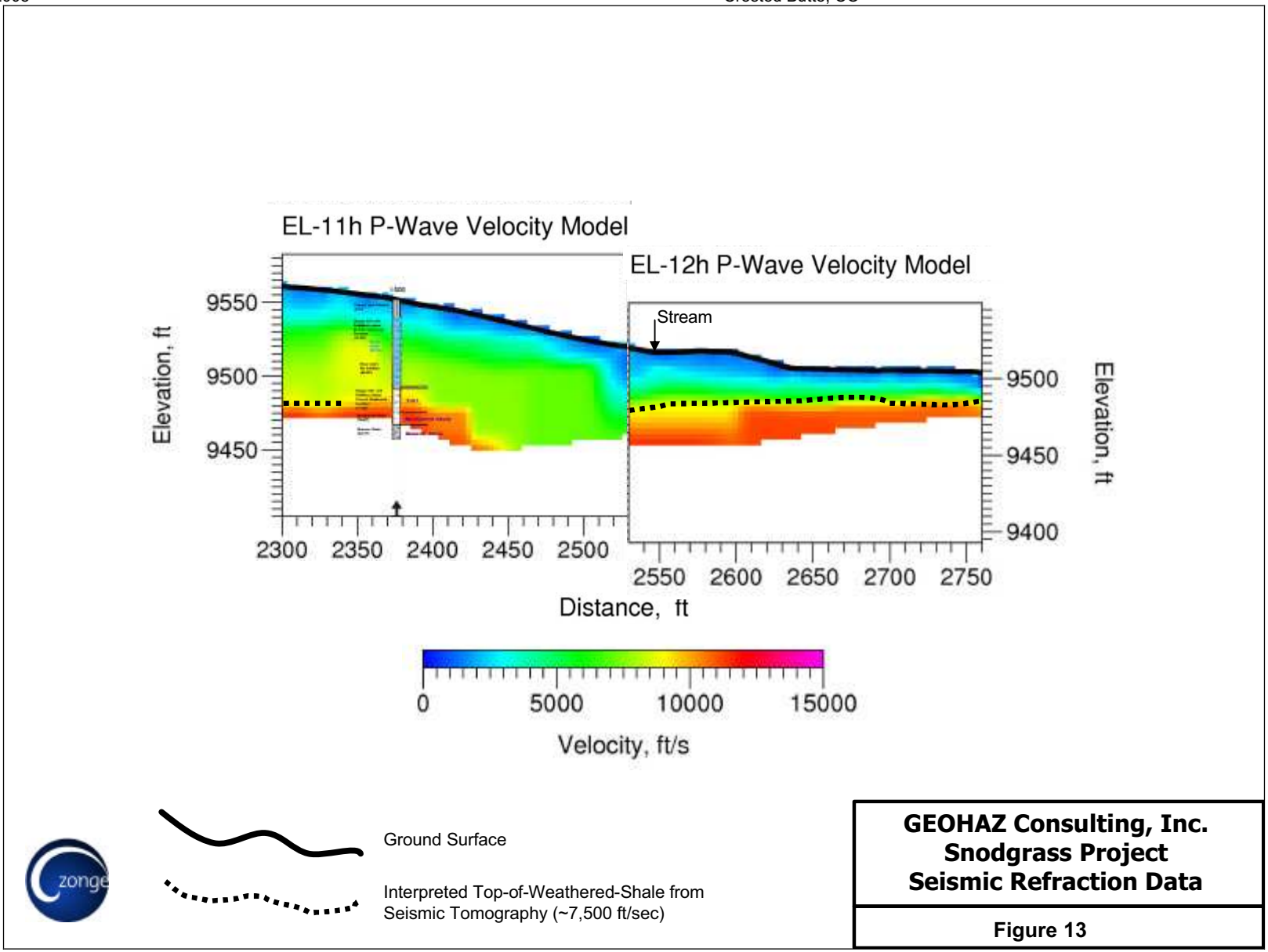

Fig. 3-28. Snodgrass, EL-11, 12 P-wave refraction tomograms

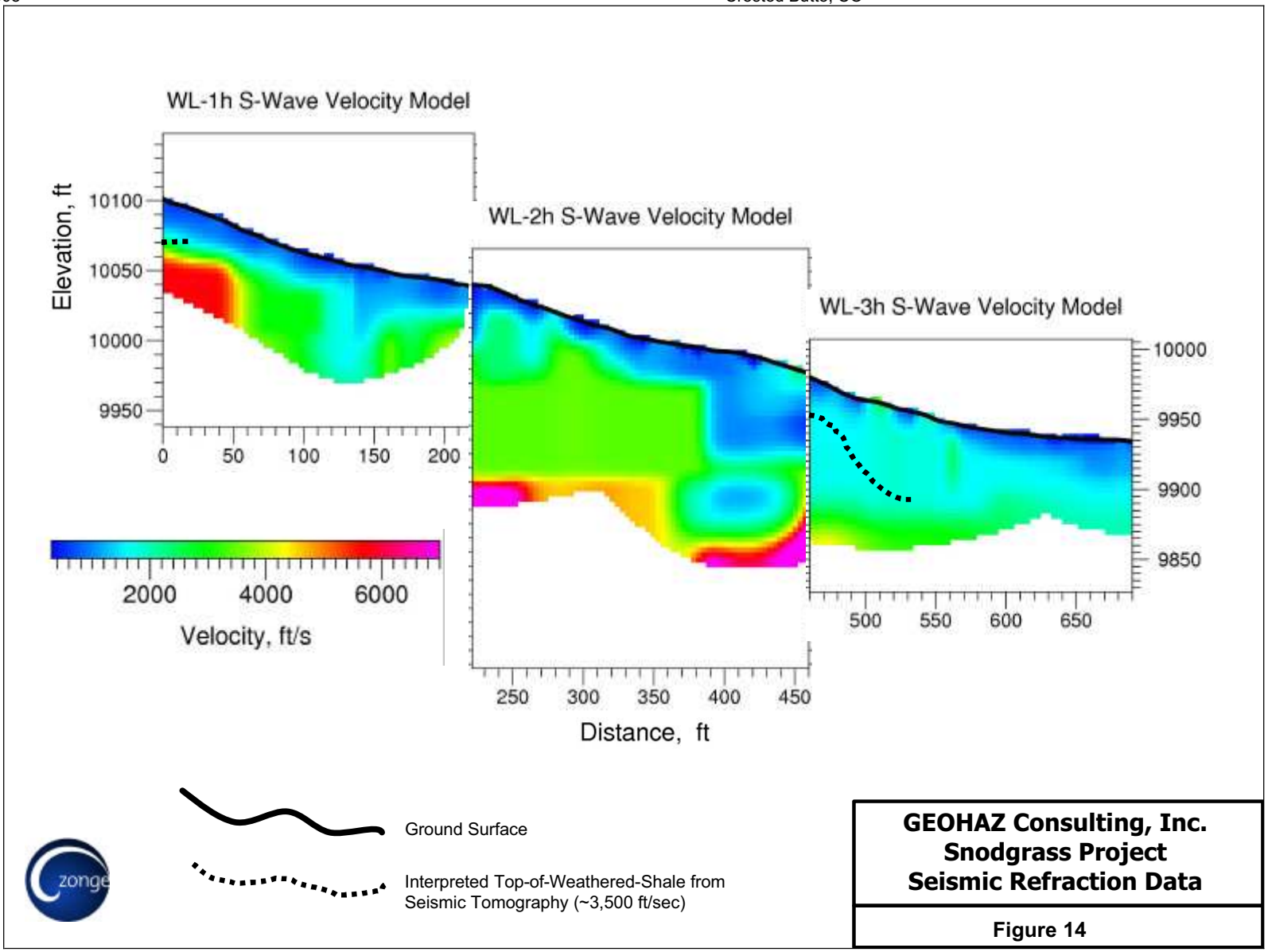

Fig. 3-29. Snodgrass, WL-1, 2, 3 S-wave refraction tomograms

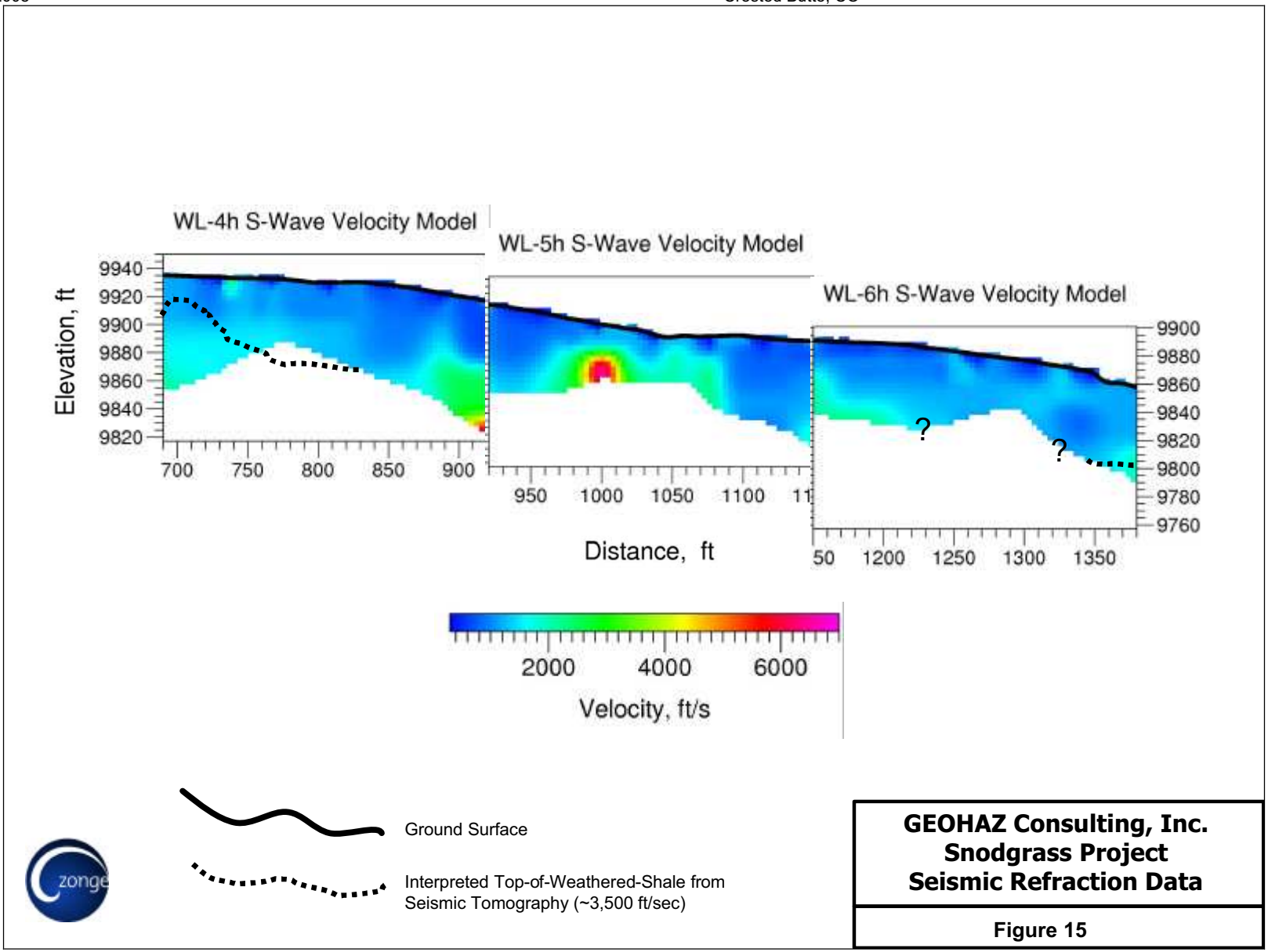

Fig. 3-29. Snodgrass, WL-4, 5, 6 S -wave refraction tomograms

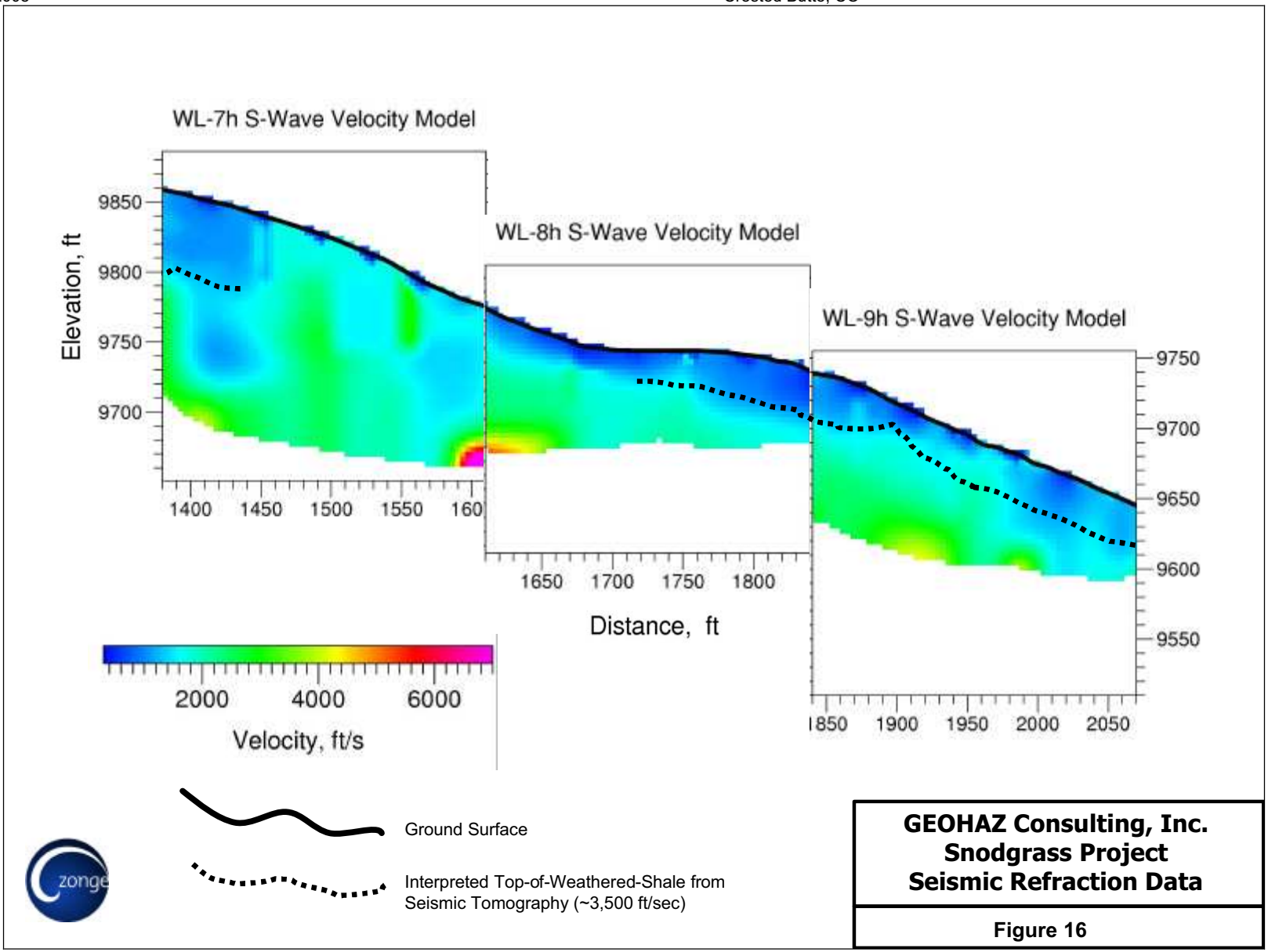

Fig. 3-30. Snodgrass, WL-7, 8, 9 S -wave refraction tomograms

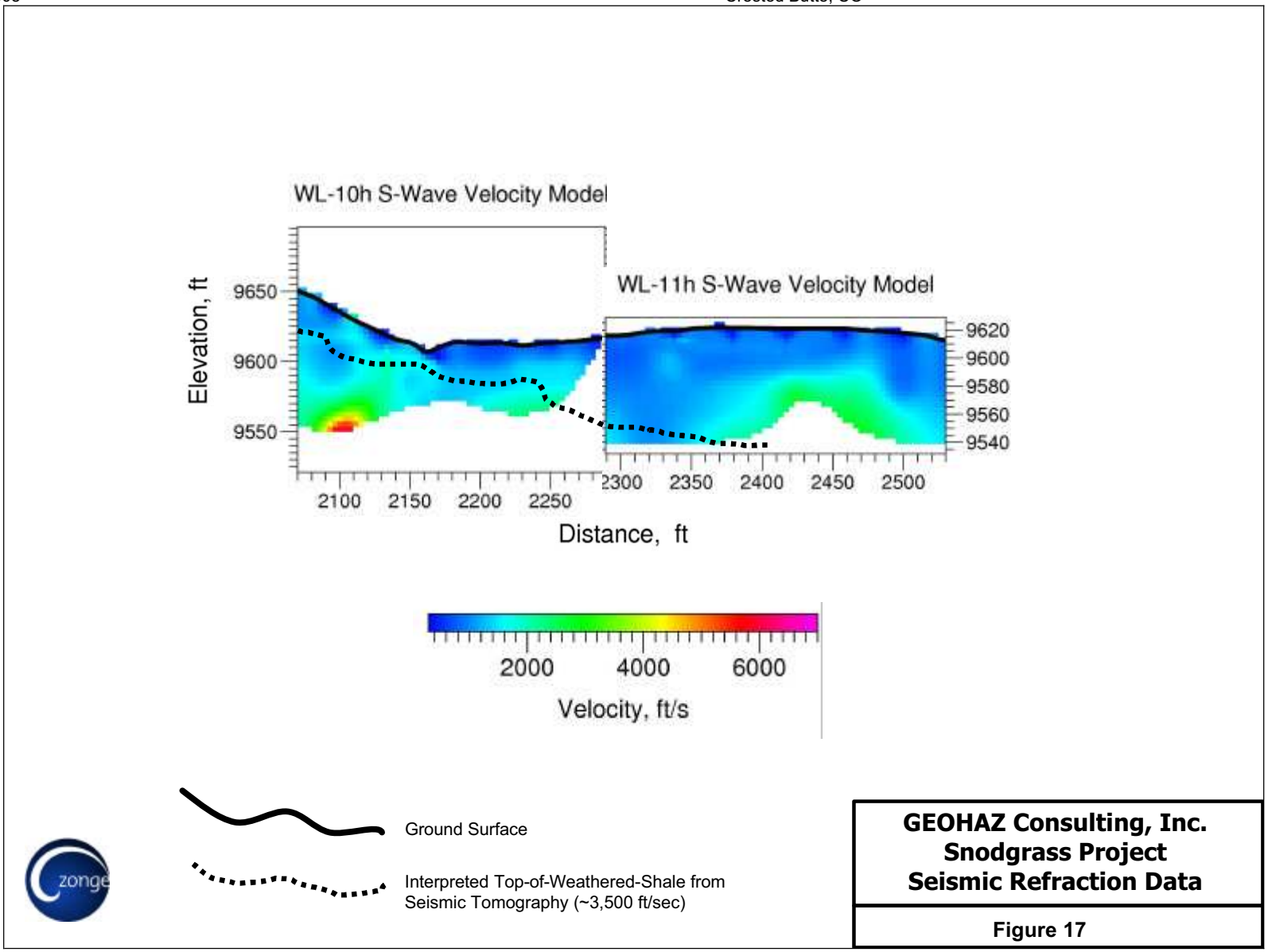

Fig. 3-31. Snodgrass, WL-10, 11 S -wave refraction tomograms

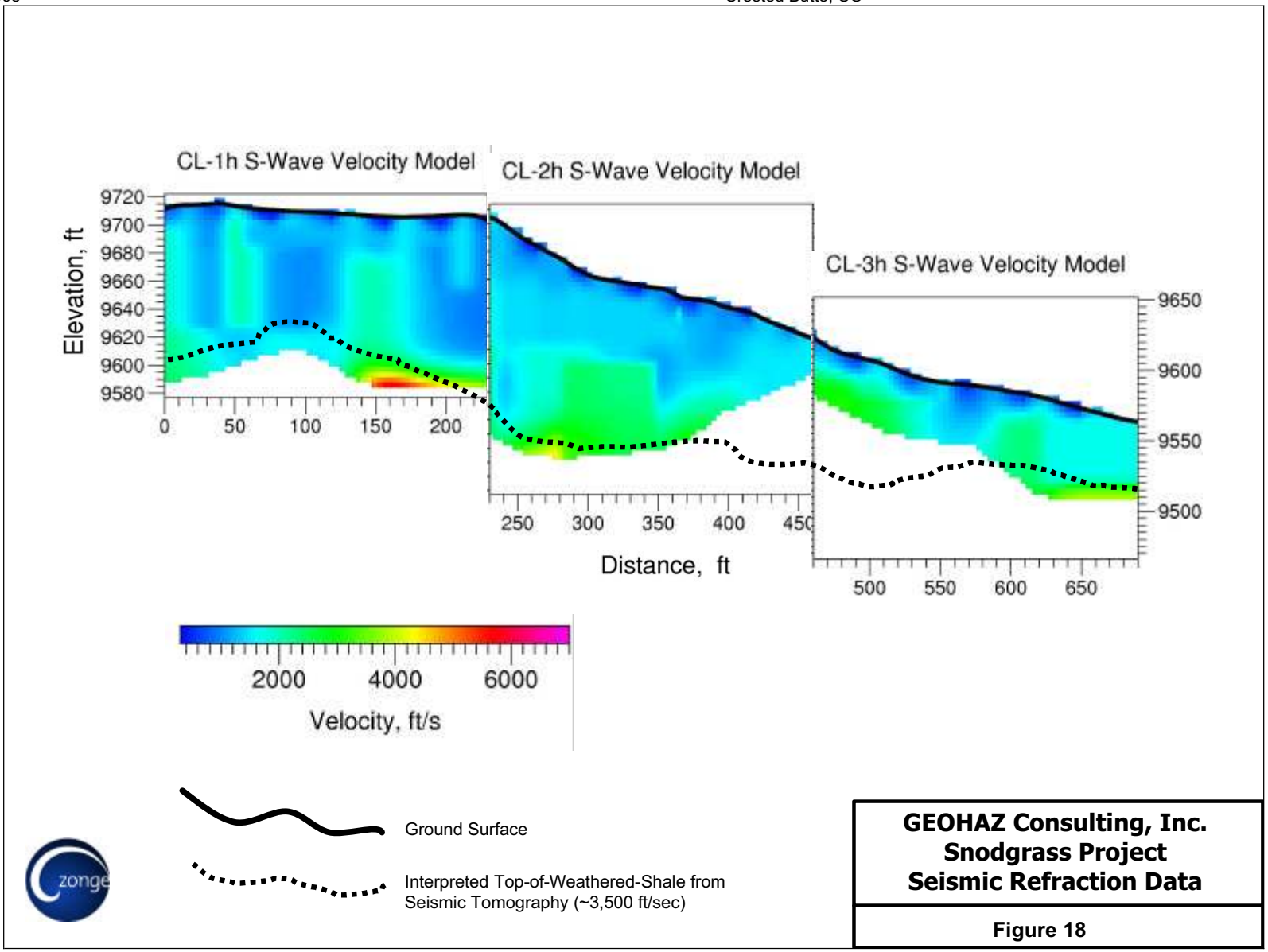

Fig. 3-32. Snodgrass, CL-1, 2, 3 S-wave refraction tomograms

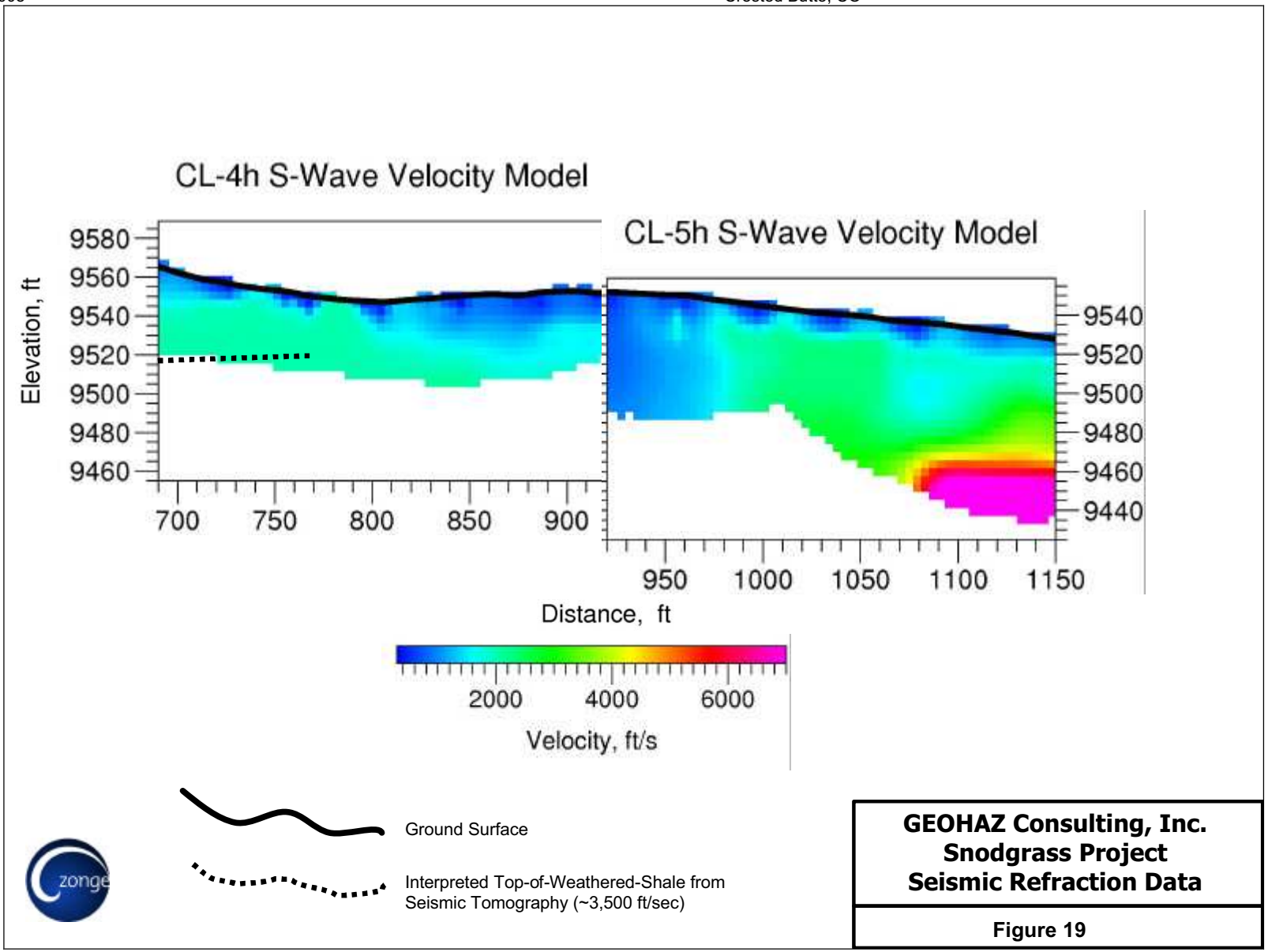

Fig. 3-33. Snodgrass, CL-4, 5, S-wave refraction tomograms

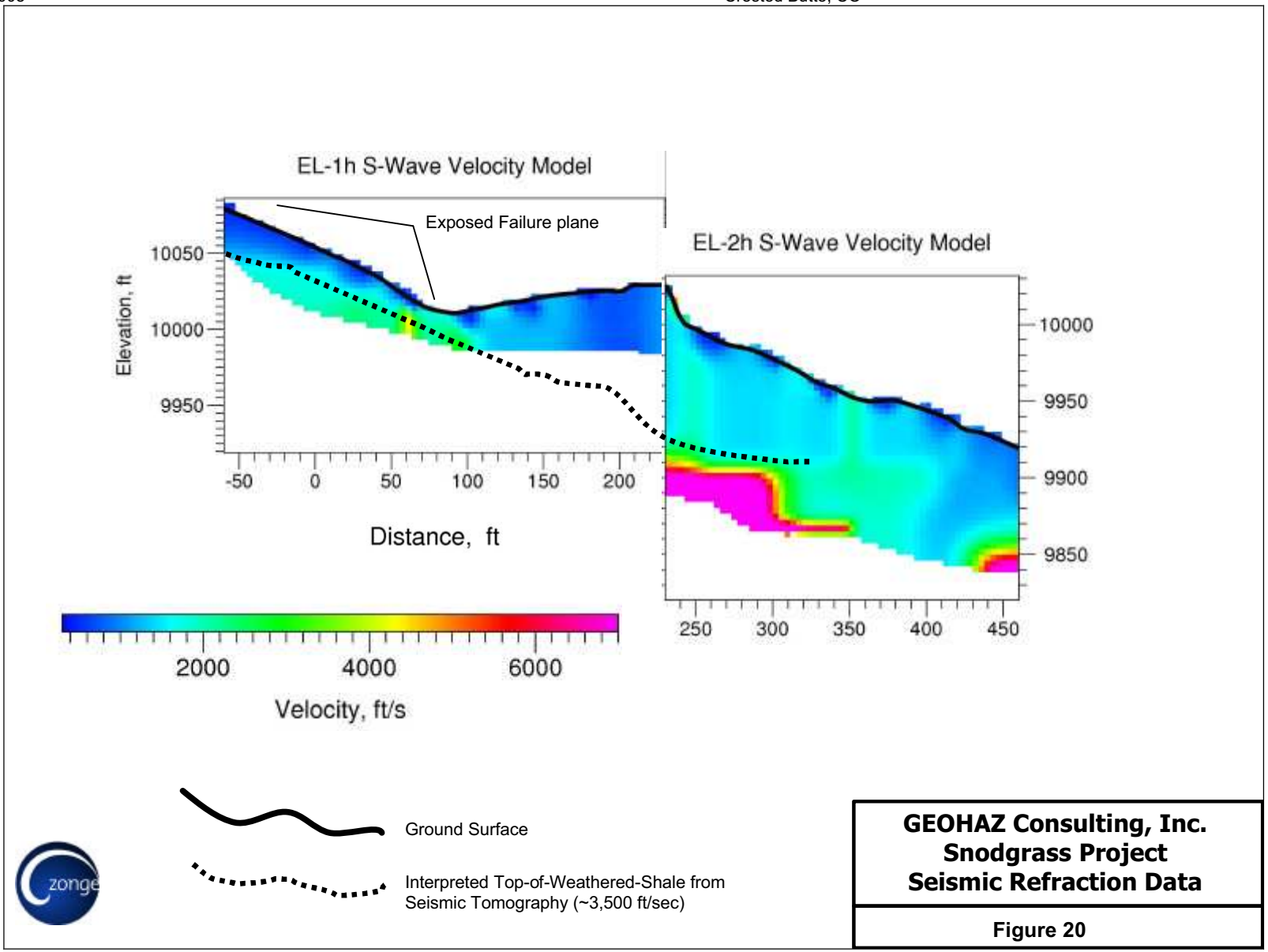

Fig. 3-34. Snodgrass, EL-1, 2 S-wave refraction tomograms

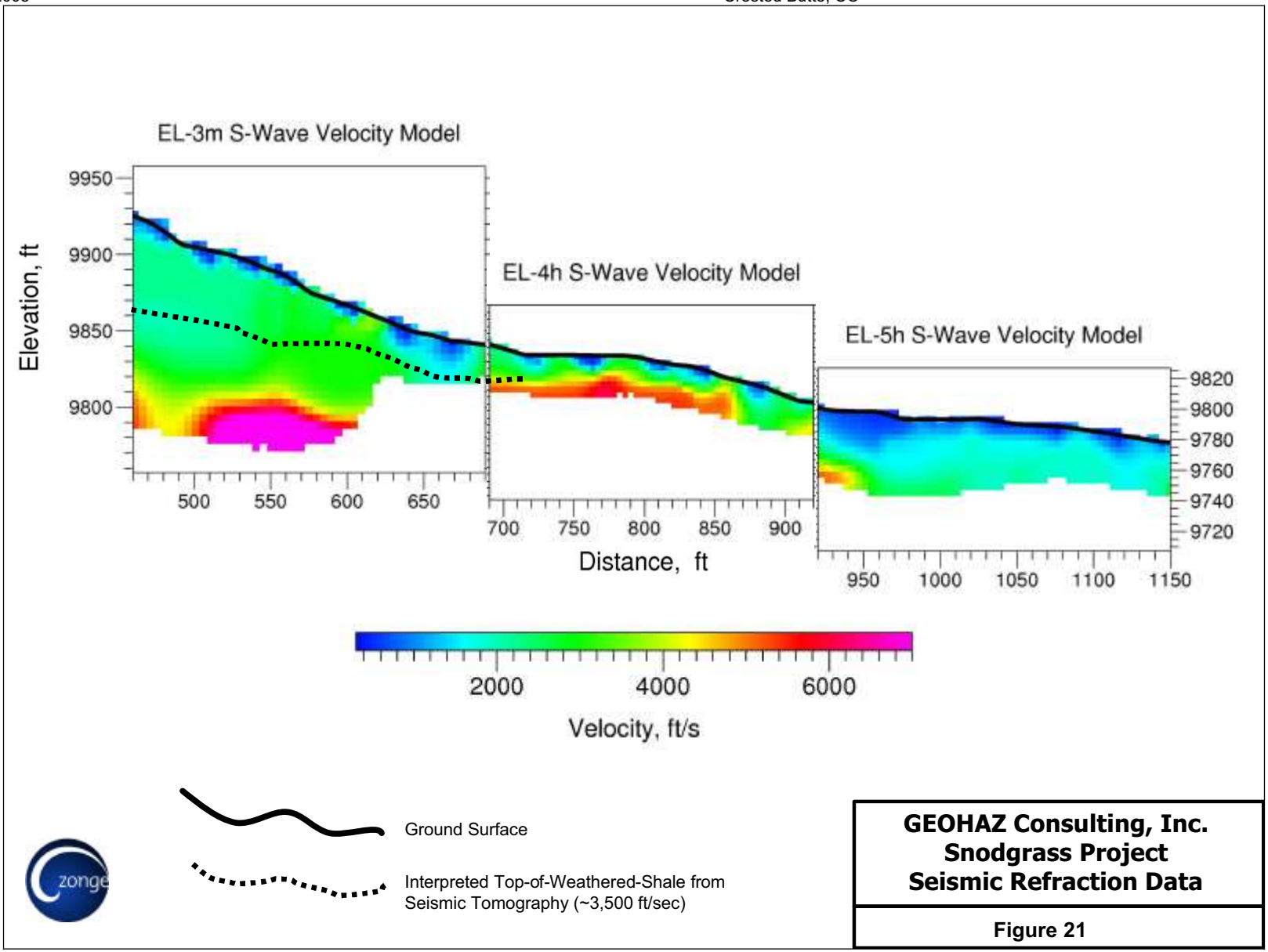

Fig. 3-36. Snodgrass, EL-3, 4, 5 S-wave refraction tomograms

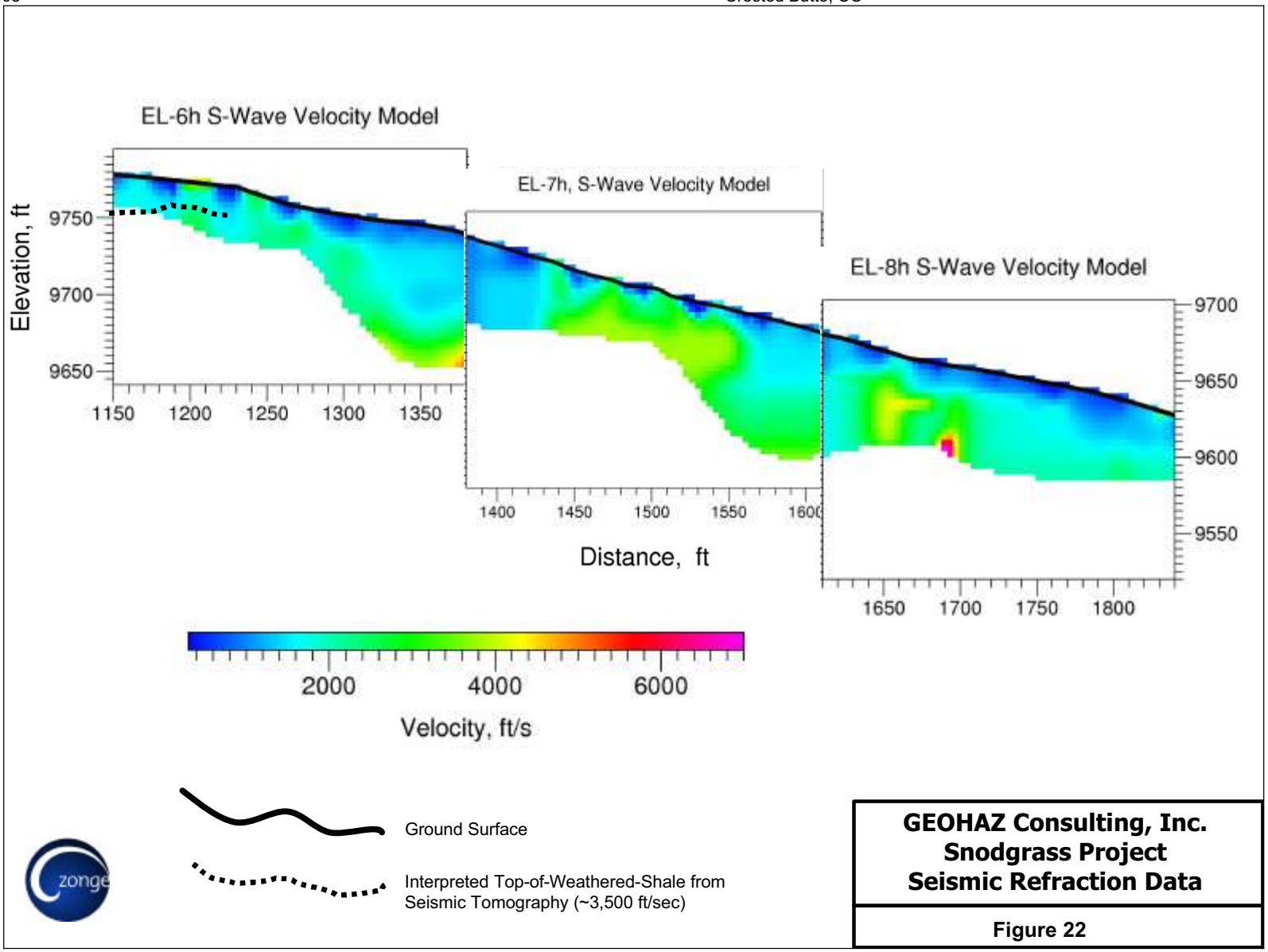

Fig. 3-37. Snodgrass, EL-6, 7, 8 S-wave refraction tomograms

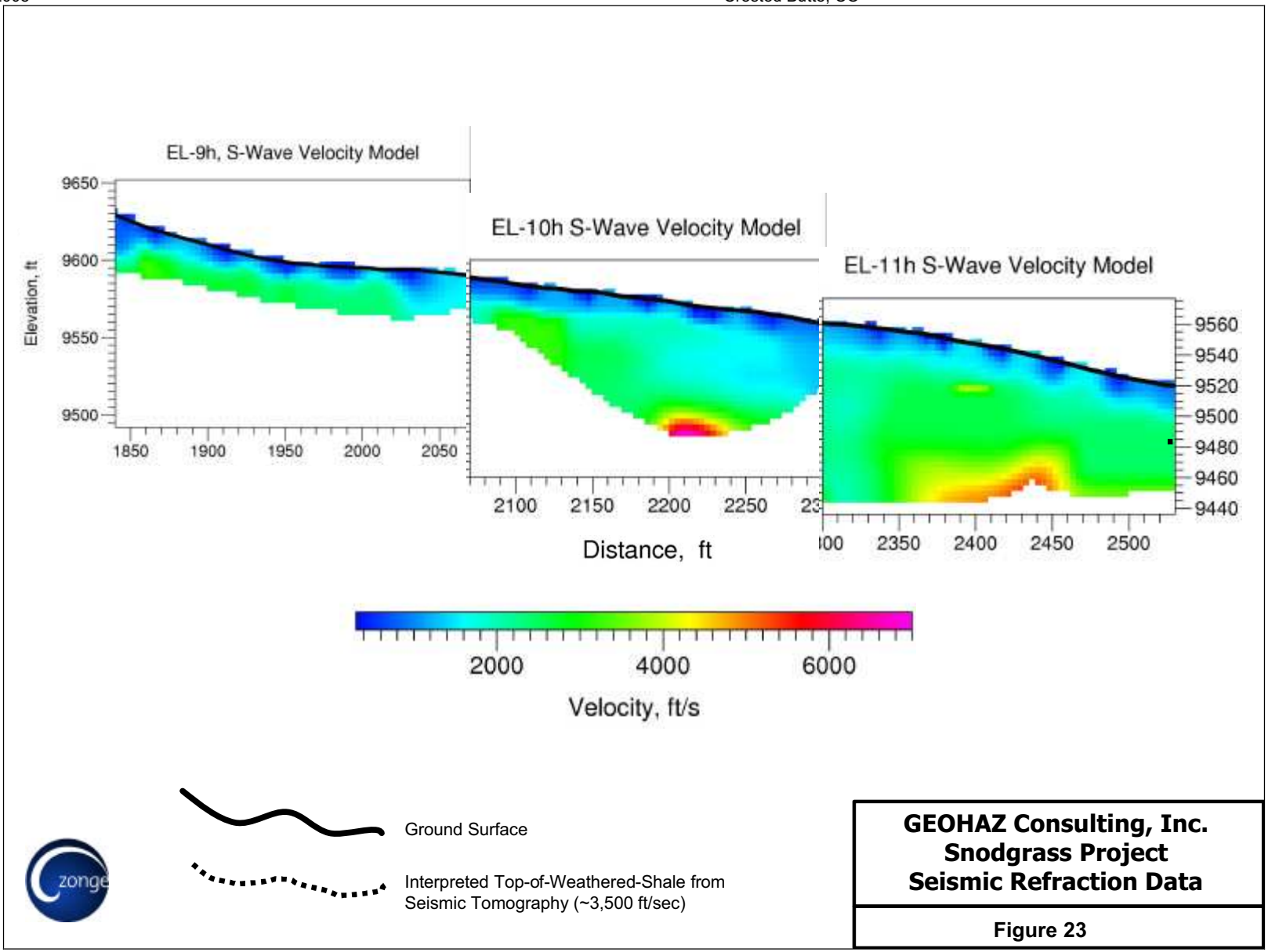

Fig. 3-38. Snodgrass, EL-9, 10, 11 S-wave refraction tomograms

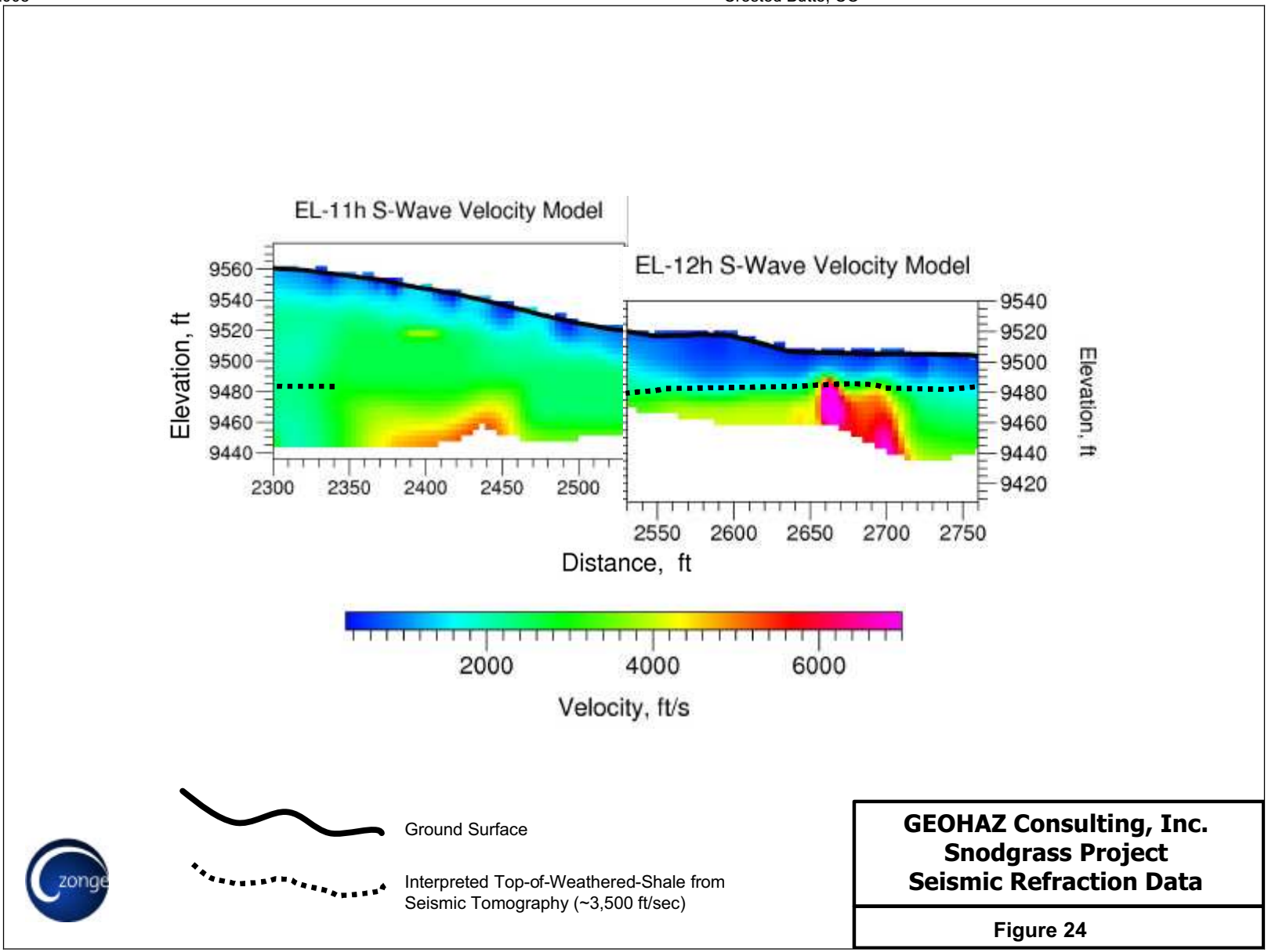

Fig. 3-39. Snodgrass, EL-11, 12 S-wave refraction tomograms.